Results in Engineering 27 (2025) 106407

Contents lists available at ScienceDirect

Results in Engineering

journal homepage: www.sciencedirect.com/journal/results-in-engineering

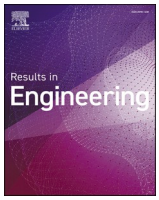

Research paper

Kinetic analysis of anaerobic coal desulfurization: Impact of particle size on sulfur content, ash and calorific value

Seshibe Makgato [a,*], Bridjesh Pappula [a], Opeyemi Oyewo [a], Tunde Yusuf [b], Naveen Kumar [c], Damian Onwudiwe [d,e], Peter Makgwane [f]

[a] Department of Chemical & Materials Engineering, College of Science, Engineering and Technology, University of South Africa (UNISA), c/o Christiaan de Wet & Pioneer Avenue, Florida Campus 1710, Johannesburg, South Africa
[b] Department of Chemistry, Faculty of Natural and Agricultural Sciences, University of Pretoria, Private Bag X20, Hatfield, PRETORIA, 0028, South Africa
[c] Department of Chemistry, Maharshi Dayanand University, Rohtak-124001, India
[d] Department of Chemistry, School of Physical and Chemical Sciences, Faculty of Natural and Agricultural Sciences, North-West University, Mafikeng Campus, Private Bag X2046, Mmabatho, 2735, South Africa
[e] Material Science Innovation and Modelling (MaSIM) Research Focus Area, Faculty of Agriculture, Science and Technology, North-West University (Mafikeng Campus), Private Bag X2046, Mmabatho, South Africa
[f] Institute for Catalysis and Energy Solutions (ICES), College of Science Engineering and Technology (CSET), University of South Africa, Private Bag X6, FL, 1710, South Africa

ARTICLE INFO

Keywords:
Sulfur
Calorific value
Ash
desulfurization
Kinetic parameters

ABSTRACT

Kinetic parameters are essential for improving desulfurization efficiency by providing insight into coal properties, reaction rates linked to ash, sulfur content, and calorific value, and for guiding process optimization. The current study develops a kinetic model and evaluates the desulfurization behavior of a bacterial consortium under anaerobic conditions for steam coal. Four particle size fractions (+4.60 mm, -4.60 + 2.30 mm, -2.30 + 1.00 mm, and -0.85 mm) were analyzed. Kinetic parameters were estimated and validated using the AQUASIM software. Over 20 days, total sulfur in the finest coal fraction (-0.85 mm) decreased from 1.45 wt.% to 0.50 wt.% corresponding to a 65.5% desulfurization efficiency under temperature condition of 23 ± 3 °C. Upon increasing the temperature to 30 ± 2 °C, sulfur removal was further improved, with the total sulfur content decreasing to 0.40 wt.%, yielding an overall removal efficiency of 72.4%. Ash in this fraction dropped from 34.2 wt.% to 23.2 wt.%, indicating a 32.2 % reduction. The calorific value improved accordingly, enhancing coal quality. Kinetic analysis showed that reaction rates increased with decreasing particle size, with the -0.85 mm fraction exhibiting the highest reaction rate constant (k_{mc} = 17.474 h^{-1}), while the +4.60 mm fraction recorded the lowest (k_{mc} = 11.105 h^{-1}). Sulfur content and ash removals followed first-order kinetics, confirming that reaction rates were concentration-dependent, while changes in calorific value followed second-order kinetics (R^2 > 97 %), suggesting more complex dependencies. These findings highlight the critical role of particle size in anaerobic biodesulfurization efficiency and provide a reliable kinetic framework for optimizing microbial coal treatment.

1. Introduction

The global demand for energy continues to sustain coal's position as a major fuel source, particularly in countries like South Africa, Poland, India, China, Australia, Russia, Germany, and the United States [1]. Coal combustion remains a dominant method of direct energy production. However, it raises significant environmental concerns due to the emission of harmful gases such as nitrogen oxides (NOx) and sulfur oxides (SOx) [2,3]. These emissions contribute to a variety of environmental and health hazards. For instance, SO_2 and H_2S are key contributors to acid rain, which can damage vegetation, disrupt soil and water chemistry, and accelerate the corrosion of infrastructure [4]. Additionally, sulfur compounds can react to form sulfates and fine particulate matter, further worsening air quality [4,5]. SOx emissions are also linked to catalyst poisoning, equipment degradation, and climate change. From a health perspective, SOx gases are toxic and associated with respiratory diseases such as asthma, bronchitis, emphysema, and cardiovascular complications, particularly affecting vulnerable populations like children [6,7]. Industrially, elevated sulfur levels degrade equipment and

* Corresponding author.
E-mail address: makgato2001@yahoo.com (S. Makgato).

https://doi.org/10.1016/j.rineng.2025.106407
Received 10 April 2025; Received in revised form 6 July 2025; Accepted 20 July 2025
Available online 21 July 2025

Nomenclature

Symbol	Description
δ_y	Approximate standard deviation of the model result
y	Arbitrary variable calculated by AQUASIM
ℓ	Model parameter by a constant
χ^2	Chi-square
A	Ash
CV	Calorific value
E	S_T reductase serves as a biocatalyst
k	Intrinsic kinetic rate constant
k_1	The reaction rate constant applies to the forward reaction
K_c	Half velocity constant (ML^{-3})
S_T	Sulfur content at time T (wt. %)
t	Time (T)
E^*Coal	Transitional bacteria
X_0	Biomass concentration (ML^{-3})
k_2	The reaction rate constant applies to the reverse reaction
k_{mc}	Maximum specific reduction rate coefficient (T^{-1})
k_3	The reaction rate constant applies to third reaction
X_t	Concentration of viable cells at time t (ML^{-3})
Z	The experimental value
Z'	The predicted value
δ_i	Standard deviations
C	Carbon (wt. %)
H	Hydrogen (wt. %)
N	Nitrogen (wt. %)
CO_3^{2-}	Carbonates (wt. %)
O	Oxygen (wt. %)
CV	Calorific Value (MJ/kg)
TM	Total Moisture (wt. %)
AM	Analytical Moisture (wt. %)
VM	Volatile matter (wt. %)
FC	Fixed Carbon (wt. %)
R and R'	Coal macromolecular groups
SEE	Standard error of estimates

increase operational costs [8].

Effective mitigation of SO_2 emissions involves controlling sulfur content at various stages—prior to combustion, during combustion through in-situ reactions, and after combustion via flue gas desulfurization [9]. Coal quality in thermal power plants is primarily evaluated based on calorific value, ash, and sulfur content. The calorific value, a key parameter, reflects the amount of chemical energy released during combustion [10]. It determines coal's suitability for power generation and its economic value [11,12]. For example, South Africa predominantly uses low-grade coal with calorific values ranging between 15 and 22 MJ/kg—significantly lower than the export-grade coal exceeding 27 MJ/kg [13]. Coal ash, defined as the residue from coal combustion, also plays a critical role in determining coal quality and price [14]. High ash levels reduce calorific value and combustion efficiency, and contribute to operational problems such as slagging, fouling, corrosion, and erosion in boilers and gasifiers [15]. Moreover, high ash content necessitates the provision of dedicated ash disposal facilities. Additionally, improper management or accidental ingress of ash into nearby water bodies can lead to significant and long-term ecological degradation [16]. Sulfur content, another problematic element in coal, affects not only environmental compliance but also the chemical behavior and commercial value of the coal [17]. As global energy policies shift toward cleaner sources, coal producers face increasing pressure to meet strict sulfur content and ash specifications [18,17].

To address these challenges, coal-cleaning technologies have gained traction. Traditional methods include physical, chemical, and microbiological techniques [19–21]. Physical cleaning relies on differences in density, magnetism, or surface properties between organic matter and sulfur-bearing minerals like pyrite [22]. However, physical methods often fall short of achieving low ash thresholds due to the intimate association of ash-forming minerals with the coal matrix [23]. Chemical desulfurization, though effective, is typically expensive, energy-intensive, and environmentally unfriendly due to its reliance on strong acids or alkalis at high temperatures and pressures, which also generate secondary pollutants like CO_2 [5,24]. Furthermore, these methods can increase coal ash by introducing extraneous minerals during treatment.

Microbial desulfurization offers a promising alternative. It operates under mild conditions, avoids harsh reagents, and can selectively target different forms of sulfur content without degrading the coal's energy potential [5,25,26]. In particular, anaerobic desulfurization uses bacteria such as sulfate-reducing bacteria (SRB) to remove sulfur compounds - including sulfates, pyritic sulfur, and organic sulfur - under oxygen-free conditions. These microbes utilize sulfur as an electron acceptor, converting sulfate into hydrogen sulfide (H_2S), which can be captured or neutralized. Anaerobic conditions are particularly effective for coals rich in pyritic and organic sulfur [27]. Particle size significantly influences desulfurization efficiency - finer coal particles offer greater surface area for microbial contact, thereby accelerating sulfur removal [5]. Anaerobic biodesulfurization has the potential to improve coal quality by lowering sulfur emissions, enhancing combustion efficiency, reducing corrosion, and making coal more acceptable in cleaner energy markets. Most previous microbial desulfurization studies have focuzed on individual bacterial strains under mesophilic and acidophilic conditions, often using coals from India or Europe [26,28,29]. However, South African coals - characterized by high ash content, low calorific value, and diverse sulfur content forms - require a more nuanced understanding of microbial consortia and kinetic behaviors. Desulfurization strategies effective for European coals, which mainly target pyritic sulfur, may not be adequate for South African coals, which exhibit a complex sulfur profile [12,30,31].

While microbial desulfurization has shown promise, existing models often emphasize optimal growth conditions without sufficiently addressing the complexities of sulfur content forms diversity or providing reliable kinetic data. Many models use broad coefficient ranges, leading to overly complex or impractical mathematical formulations [20,32,33]. There remains a significant gap in the literature regarding the kinetic parameters specific to coals with multiple sulfur forms. Therefore, this study aims to develop a robust kinetic model to describe the desulfurization and deashing behavior of steam coal using an anaerobic bacterial consortium. The investigation focuses on the impact of particle size on sulfur content and ash removal, and evaluates changes in calorific value. Four particle size fractions (+4.60 mm, −4.60 + 2.30 mm, −2.30 + 1.00 mm, and −0.85 mm) were analyzed. Kinetic parameters were estimated and validated using the AQUASIM software, with the goal of optimizing microbial desulfurization processes tailored to South African coal characteristics.

2. Materials and methods

2.1. Coal samples and preparation

Coal samples were collected from a local power station in Lephalale, Limpopo province, South Africa. To obtain a representative sample, the coal samples were thoroughly combined and distributed. The Ro-Tap® Testing Sieve Shaker screened the samples utilizing five distinct size fractions for five minutes, using sieves of −0.85 mm, −1.00 + 0.85 mm, −2.30 + 1.00 mm, −4.60 + 2.30 mm and +4.60 mm.

2.2. Basal mineral medium

Basal mineral medium (BMM) was prepared by dissolving (in 1 L distilled water): 1.013 g/L NH_4Cl; 0.620 g/L $NaH_2PO_4{\cdot}2H_2O$; 2.5 g/L K_2HPO_4; 0.0103 g/L $MgSO_4{\cdot}7H_2O$; 0.00425 g/L $CaCl_2{\cdot}2H_2O$; and 0.00085 g/L $FeCl_3{\cdot}3H_2O$. The BMM was adjusted by adding 1 mL of trace metals prepared by dissolving (in 1 L distilled water): 0.243 g/L $FeCl_3{\cdot}6H_2O$; 0.060 g/L $MnCl_2{\cdot}2H_2O$; 0.041 g/L $ZnCl_2$; 0.026 g/L $CuCl_2{\cdot}2H_2O$; 0.036 g/L $CoCl_2{\cdot}2H_2O$; 0.015 g/L $Na_2B_4O_7{\cdot}10H_2O$; 2.205 g/L $Na_3C_6H_5O_7$; 0.026 g/L $(NH_4)_6Mo_7O_{27}{\cdot}4H_2O$; 5.104 g/L KH_2PO_4; 3.105 g/L $NaH_2PO_4{\cdot}H_2O$; 1.980 g/L $(NH_4)_2SO_4$; 18.450 g/L NH_4Cl; 2.205 g/L $CaCl_2{\cdot}2H_2O$; 3.049 g/L $MgCl_2{\cdot}6H_2O$; and 0.025 g/L $NiCl_2{\cdot}6H_2O$), and 5 mL of a trace vitamin stock solution (g/L): 0.004 biotin; 0.004 folic acid; 0.02 pyridoxine hydrochloride; 0.01 riboflavin; 0.01 thiamin; 0.01 nicotinic acid; 0.0002 B_{12}; 0.01 p-aminobenzoic acid; and 0.01 thiotic acid). MERCK Chemicals supplied all the chemicals with purity levels greater than 99 %.

2.3. Microbial desulfurization culturing

A diverse culture of sulfur-reducing bacteria was prepared out of coal samples used for electricity production. Coal samples were taken from the mills of the power plant using auto-sampling. The start-up culture was prepared by cultivating Luria-Bettani (LB) broth overnight at 32 °C. A shaker incubator was used to incubate the bacterial culture at 30 °C, 125 rpm. After 24 h, the bacterial culture was filtered using a weighted glass-fiber filter (Whatman, GF/A, diameter of 90 mm and pore size of 1.2 m) and inoculated the reactor for biodesulfurization experiments. Biolab (Midrand, South Africa) supplied the LB broth and LB agar used to grow colony-forming units.

2.4. Flow chart of desulfurization process and process parameters

Fig. 1 illustrates the step-by-step biodesulfurization process of coal with high sulfur content and ash. The process begins with coal grinding into five particle size fractions (+4.60 mm, -4.60 + 2.30 mm, -2.30 + 1.00 mm, -1.00 + 0.85 mm, and -0.85 mm). The -1.00 +0.85 mm particle size fraction was excluded, as its proximate and ultimate analysis results were within the repeatability error range of the -0.85 mm fraction. The ground coal was then mixed with nutrients to form a slurry, which is subsequently inoculated with an anaerobic bacterial consortium. This mixture underwent temperature-controlled anaerobic incubation, leading to sulfur content reduction. The coal was then separated and washed to remove bacterial cells and by-products, resulting in biodesulfurized coal with reduced sulfur content and ash and enhanced calorific value.

Table 1 summarizes the key parameters of the desulfurization process: coal particle sizes used were −0.85 mm, −2.30 + 1.00 mm, −4.60 + 2.30 mm, and +4.60 mm; incubation temperatures ranged from 23 ± 3 °C to 30 ± 2 °C; the incubation period spanned from 0 to 20 days; and the inoculum used was an anaerobic bacterial consortium.

2.5. Experimental set-up

The 500-mL continuously stirred Erlenmeyer flask was used for the desulfurization tests. 250 mL of a group of bacteria with coal sample of 200 g was used to start up the reactor. A magnetic stirrer operating at 200 rpm homogenized the media to maintain fully stirred tank reactor (CSTR). Five possible size fractions of −0.85 mm, −1.00 + 0.85 mm, −2.30 + 1.00 mm, −4.60 + 2.30 mm and +4.60 mm were considered. However, the particle size fraction of −1.00 to +0.85 mm was disregarded primarily because its proximate and ultimate analyses fell within the repeatability error range for the −0.85 mm fraction. A total of three operating conditions were applied to the reactor: uninoculated (30 ± 2 °C), inoculated (23 ± 3 °C) and uninoculated (23 ± 3 °C) for 20 days. For analysis preparation, coal samples of 20 g were withdrawn from the biodesulfurization experiments. Coal was autoclaved at 103 Pa (gauge) for 15 min to sterilize it for use in research and eliminate any innate microorganisms. To remove any microorganisms, the treated coal samples were subjected to vacuum filtration using a peristaltic pump. Coal samples that had been treated were dried in a protea drying oven at 30 ± 2 °C and examined the following day. Fig. 2 shows a schematic of the system for a microbial desulfurization reactor.

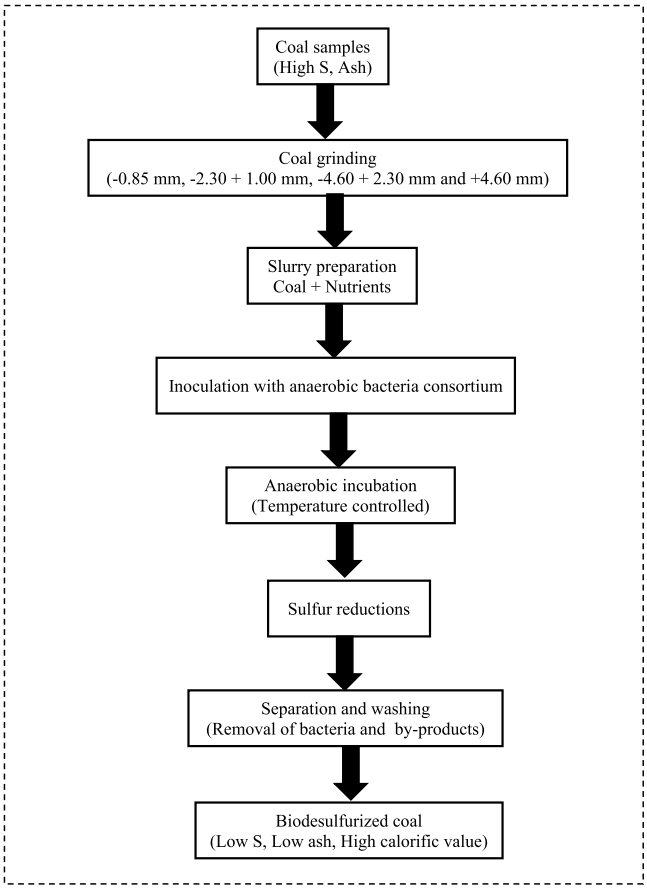

Fig. 1. Flow chart of desulfurization process.

Table 1
Process parameters.

Parameter	Value
Coal particle size (mm)	−0.85 mm, −2.30 + 1.00 mm, −4.60 + 2.30 mm and +4.60 mm
Incubation temperature (°C)	23 ± 3 °C to 30 ± 2 °C
Incubation Time (Day)	0 – 20
Inoculum Type	Anaerobic bacterial consortium

2.6. Phylogenetic analyses

Phylogenetic analyses were conducted by using an NCBI-BLAST search to match 16S rRNA sequences to database sequences that were already accessible. GenBank was used to find the related taxa. The various alignments were carried out using the CLUSTAL X software. The 16S rRNA gene sequences were modified using the BioEdit program. The MEGA 3 program created phylogenetic trees using the neighboring-joining and maximum-parsimony techniques. The degree of similarity between the clones and other known sulfate-reducing species was determined by comparing their rRNA gene sequences.

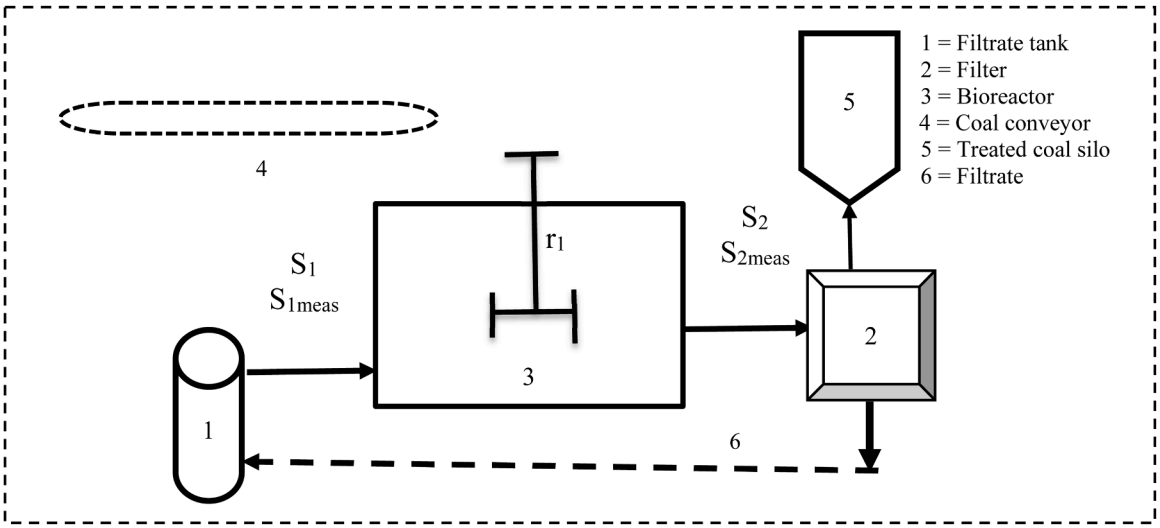

Fig. 2. A simplified representation of the microbial desulfurization process.

2.7. Ultimate analysis and calorific value determination

The LECO-932 CHNS Analyzer was utilized to determine ultimate analyses, including carbon, hydrogen, and nitrogen, by ISO 12902 [34] standard procedure. The calorific value (CV) of coal samples was determined using the ISO 1928 [35] method after the samples were burned in a bomb calorimeter.

2.8. Analysis of sulphur forms in coal samples

MAE instrument was used for determining forms of sulfur content in coal samples following ISO 157 [36] standard procedure and the organic sulfur was calculated by difference from the total sulfur.

2.9. Proximate analysis

In proximate analysis, parameters like fixed carbon (by difference), moisture content, ash and volatile matter are determined. Coal consists of mineral as well as non-volatile matter, which includes fixed carbon (FC). Moreover, the proximate analysis estimates the FC by deducting the total percentages of volatile matter, moisture and ash from 100. As a result, the FC accumulates all errors from testing other variables such as moisture, ash and volatiles. Water content of coal was measured by the mass lost from a certain volume of dried coal in an oven at 150 ± 5 °C with forced air flow according to ISO-11,722 [37]. Ash is the residue left after incineration has removed all organic matter. A furnace that maintains a temperature range of 815 ± 10 °C was used to determine the ash using the ISO 1171 [38] standard procedure. The carbolite furnace, operating at a temperature of 100 °C, determined volatile matter in accordance with ISO 562 [39] standard procedure.

2.10. AQUASIM 2.0 software simulation analysis

AQUASIM uses the implicit (backward differencing) variable-step as well as the variable-order Gear integration technique for data simulation. For this, a numerical integration system for time-dependent ordinary and partial deferential equations was used allowing for the simultaneous solution of the algebraic equations. Conservative finite deference techniques for the spatial discretization of partial deferential equations were used. Furthermore, the DASSL algorithm can solve the nonlinear system of algebraic equations using the whole or labelled Jacobian matrix from Eq. (1):

$$\frac{\partial \widehat{p}}{dt} = \frac{\partial \widehat{j}}{\partial z} + \widehat{r} \tag{1}$$

Eq. (1) is discretized as Eq. (2):

$$\frac{d}{dt}\widehat{p}(x_i, t) = \frac{\widehat{j}_{num}(x_{i+0.5}, t) - \widehat{j}_{num}(x_{i-0.5}, t)}{x_{i+0.5} - x_{i-0.5}} + \widehat{r}(x_i, t) \tag{2}$$

$$\underline{J} = \frac{\partial F}{\partial y} \tag{3}$$

$$\underline{J} = \begin{bmatrix} \frac{\partial f_1}{\partial x_1} \cdots\cdots \frac{\partial f_1}{dy} \\ \frac{\partial f_2}{\partial x_2} \cdots\cdots \frac{df_2}{dy} \end{bmatrix} \tag{4}$$

2.11. Kinetic parameter estimation

The kinetic equations for a customized Monod-type equation were developed and fitted the experimental results to sulfur content, coal ash and calorific value. Typically, biodegradation processes use a Monod-type kinetic equation to describe microbial growth or reaction rates. The numerical evaluation of the mass balance in AQUASIM 2.0 was done using the fourth-order Runge-Kutta (RK-4) method. By employing a simplex approach implemented in AQUASIM, using a method that minimizes the Chi-square (χ^2) values comparing the actual and model data, we were able to calculate the parameters. AQUASIM estimates model parameters using constant variables by minimizing Eq. (4) under certain constraints ($\ell_{min,i} \le \ell_i \le \ell_{max,i}$). This formula is defined as the accumulated squared errors between observed data and model predictions. We use either the simplex approach or the secant algorithm to find the minimum solution to Eq. (5):

$$x^2(\ell) = \sum_{i=1}^{n} \left[\frac{U_{meas,i} - U_i(\ell)}{\alpha_{meas,i}} \right]^2 \tag{5}$$

2.12. Analyzing the estimated parameters' sensitivity

Integrating identifiability analysis as well as uncertainty analysis, the sensitivity analysis of AQUASIM was solved. An identifiability analysis is conducted using AQUASIM to assess whether the model parameters can be individually estimated from the available data and to evaluate the associated parameter uncertainty estimations. Through parameter esti-

mation, the parameter standard error was made use of along with correlation coefficient. Equations 6 to 9 are distinguished using AQUASIM.

$$\delta_{y,\ell}^{a,a} = \frac{\partial y}{\partial \ell} \tag{6}$$

$$\delta_{y,\ell}^{r,a} = \frac{1}{y}\frac{\partial y}{\partial \ell} \tag{7}$$

$$\delta_{y,\ell}^{a,r} = p\frac{\partial y}{\partial \ell} \tag{8}$$

$$\delta_{y,\ell}^{r,r} = \frac{p}{y}\frac{\partial y}{\partial \ell} \tag{9}$$

where y is the arbitrary variable found using AQUASIM and ℓ is the model parameter

$$\delta_y = \sqrt{\sum_{i=1}^{m}\left(\frac{\partial y}{\partial \ell_i}\right)^2 \delta_{\ell_i}^2} \tag{10}$$

The error contribution made by each parameter is provided as:

$$\delta_{y\ell}^{err} = \frac{\partial y}{\partial \ell}\delta_\ell \tag{11}$$

AQUASIM 2.0 is used to calculate Equations (6) – (9) and (11) utilizing the derivatives:

$$\frac{\partial y}{\partial \ell_i} \approx \frac{y(\ell_i + \Delta\ell_i) - y(\ell_i)}{\Delta\ell_i} \tag{12}$$

2.13. Statistical variation

The standard error of an estimate (SEE) is a way to measure how accurate predictions or models are. This is shown in Eq. (13).

$$E = \sqrt{\frac{\sum (Z - Z')}{N}} \tag{13}$$

3. Results and discussions

3.1. Raw coal proximate analysis, ultimate analysis and calorific value

Table 2 presents the results for raw coal calorific value, ultimate analysis, and proximate analysis. The carbon content, which is the primary energy source during coal combustion, ranges from 50.84 to 52.73 wt %, indicating a moderate level of carbon in the coal. Hydrogen content, essential for energy production as it contributes to water formation during combustion, varies between 3.33 and 3.42 wt %. This range is typical for coal but generally lower than the carbon content [40]. Oxygen content, which plays a key role in ignition, generally varies inversely with carbon content [40] and is found here between 4.34 and 5.76 wt %. According to Makgato and Chirwa [30], coal samples with oxygen levels in this range are prone to spontaneous combustion, thus requiring extra precautions during storage and transport [41].

In contrast, nitrogen content—ranging from 0.98 to 1.02 wt %—does not correlate with coal rank and does not influence spontaneous combustion. However, during combustion, nitrogen from both the coal's organic matter and atmospheric air forms nitrogen oxides (NO and NO_2), collectively known as NOx, which are significant environmental pollutants contributing to acid rain, similar to SOx [42].

Based on sulfur content, coal is classified into several categories, including ultra-low to high sulfur coal [22]. The observed sulfur content of 1.41 to 1.45 wt % places this coal in the medium sulfur category. This sulfur primarily originates from the plant material incorporated during peat formation and sulfate from seawater that flooded the peat swamps [43]. With an ash ranging from 34.0 to 34.6 wt %, the coal is classified as high ash, which is generally less desirable due to its substantial impact on boiler design and performance - necessitating larger mills and increased milling capacity [22].

The calorific value of the coal samples was determined to be 20.3 MJ/kg, representing the energy released upon complete combustion, and aligns well with previous findings by Mollo et al. [42]. Total moisture content ranged from 3.02 to 3.06 wt %, which is favorable since excessive moisture can lead to self-ignition during transportation and storage [41]. Additionally, high moisture content can lower furnace temperature and reduce boiler efficiency, making low-moisture coal preferable for combustion [41].

Volatile matter content ranged between 24.1 and 24.6 wt %. Coal with higher volatile matter ignites more easily, which necessitates careful handling during storage and transport [41]. Fixed carbon content ranged from 37.76 to 38.18 wt %. Efficient combustion of fixed carbon requires an adequate supply of air, sufficient temperature, and residence time [41].

Table 3 displays the distribution of various sulfur content forms—sulfide sulfur, sulfate sulfur, organic sulfur, pyritic sulfur, and total sulfur—in coal samples sorted by particle size. Organic sulfur was calculated by subtracting the combined amounts of pyritic, sulfide, and sulfate sulfur from the total sulfur content [44]. The results (expressed in wt. %) are consistent across the four particle size fractions, showing only minor variations. This suggests that particle size has a negligible effect on the distribution of sulfur content forms in these coal samples. Organic and pyritic sulfur are the predominant forms, together accounting for over 85 % of the total sulfur content. Meanwhile, sulfide and sulfate sulfur levels remain steady at 0.16 wt. % and 0.03 wt. % across all particle sizes. These findings correspond closely with those of Nath et al. [45], who observed that organic and pyritic sulfur dominated coal samples in roughly comparable amounts, with sulfate sulfur present in much lower concentrations. Organic sulfur content varies slightly between 0.606 and 0.624 wt. %, peaking in the finest fraction (−0.85 mm), while pyritic sulfur shows minor fluctuations, ranging from 0.595 to 0.638 wt. %. This data is critical for informing environmental

Table 2
Raw coal proximate and ultimate analysis (adb).

Analysis	−0.85 mm	−2.30 +1.00 mm	−4.60 + 2.30 mm	+4.60 mm
Ultimate Analysis				
C (wt. %)	51.98	51.62	50.84	52.73
H (wt. %)	3.37	3.33	3.34	3.42
N (wt. %)	1.00	1.01	0.98	1.02
S_T(wt. %)	1.45	1.41	1.44	1.43
O (wt. %) (by difference)	4.98	5.10	5.76	4.34
Calorific Value (MJ/kg)	20.3	20.3	20.3	20.3
TM (wt. %)	3.02	3.03	3.04	3.06
Proximate Analysis				
Ash (wt. %)	34.2	34.5	34.6	34.0
VM (wt. %)	24.6	24.5	24.6	24.1
FC (wt. %) (by difference)	38.18	38.00	37.76	37.84

C - Carbon; H – Hydrogen; N – Nitrogen; S_T =Total Sulfur; CO_3^{2-} – Carbonates; *O* = Oxygen; CV = Calorific Value; TM = Total Moisture; AM - Analytical Moisture; VM – Volatile matter; FC – Fixed Carbon.

Table 3
Analysis of sulphur forms in coal samples (wt. %).

Particle size	Sulfide sulfur	Sulfate sulfur	Organic sulfur	Pyritic sulfur	Total sulfur
−0.85 mm	0.16	0.03	0.624	0.638	1.45
−2.30 + 1.00 mm	0.16	0.03	0.606	0.595	1.41
−4.60 + 2.30 mm	0.16	0.03	0.619	0.638	1.44
+4.60 mm	0.16	0.03	0.615	0.624	1.43

compliance measures and sulfur reduction strategies during coal utilization.

The process chemistry of anaerobic sulfur removal involves microbial metabolism under oxygen-free (anaerobic) conditions, where bacteria use sulfur compounds as electron acceptors in their energy-generating pathways. The detailed breakdown of the anaerobic sulfur removal process chemistry for various sulfur content forms is shown in the following overall reactions:

Sulfate reduction by SRB:

$$SO_4^{2-} + 4H_2 + H^+ \rightarrow H_2S + 4H_2O$$

Reduction of pyrite:

$$FeS_2 + H_2 \leftarrow FeS + H_2S$$

Formation of ferrous sulfide: $Fe2^+ + H_2S \rightarrow FeS\downarrow + 2H^+$

Enzymatic hydrolysis and reduction of organic sulfur:

$$R - S - R' + H_2 \rightarrow R - H + R' - H + H_2S$$

Where R and R' are coal macromolecular groups

3.2. Experimental results for desulfurization of coal

3.2.1. The effect of desulfurization on sulfur content

Table 4 presents the effect of desulfurization treatment on the sulfur content, ash, and calorific value of coal samples across different particle sizes. The data reveal that desulfurization was most effective in finer particles, with temperature also playing a key role in enhancing sulfur reduction. For the finest particle size fraction (−0.85 mm), total sulfur content decreased significantly from 1.45 wt. % to 0.50 wt. % over 20 days, corresponding to a removal rate of 65.5 %. When the incubation temperature increased from 23 ± 3 °C to 30 ± 2 °C, sulfur content was further reduced to 0.40 wt. %, yielding a total reduction of 72.4 %. This enhanced desulfurization performance is attributed to optimal conditions for bacterial growth at elevated temperatures [46]. In contrast, control experiments at 23 ± 3 °C without microbial inoculation showed only a modest decline to 1.27 wt. % (a 12.4 % reduction), indicating limited activity by indigenous microbes. The −2.30 + 1.00 mm fraction also exhibited effective sulfur removal, dropping from 1.41 wt. % to 0.65 wt. %, a reduction of 53.9 %. At 30 ± 2 °C, the total sulfur further declined to 0.60 wt. %, amounting to a total removal of 57.4 %. Similarly, for the −4.60 + 2.30 mm fraction, sulfur content fell from 1.45 wt. % to 0.73 wt. %, a 49.7 % reduction, with additional temperature-induced reduction to 0.66 wt. %, bringing the total removal to 54.5 %. Control tests in this size range showed only a small decrease to 1.29 wt. %, again pointing to limited native microbial activity [46]. For coarse particles (+4.60 mm), desulfurization was less pronounced. Total sulfur decreased from 1.45 wt. % to 1.10 wt. %, a 24.1 % reduction, with a further drop to 1.03 wt. % at higher temperatures (28.9 % total removal). Control experiments showed minimal sulfur loss to 1.35 wt. %, supporting the observation that natural desulfurization is ineffective without microbial augmentation [46]. The reduced sulfur removal efficiency in larger particles is attributed to several factors, including reduced surface area, limited mass transfer, poor stirring, and insufficient contact between bacteria and coal surfaces. These limitations are consistent with the findings of Yu et al. [47], who reported that larger particles present challenges due to their lower free sulfur content and poor solubility. Moreover, microbial solutions interacting with large coal particles face significant resistance to mass transfer [48]. Interestingly, enhanced desulfurization in larger particles began once enough coal was removed during sampling to allow for more effective stirring. This underscores the importance of particle size in influencing sulfur accessibility, oxidation kinetics, and microbial metabolism.

Overall, the results support the economic and environmental case for using finer coal particles in desulfurization strategies. Smaller particle sizes offer a greater surface area, which enhances microbial contact and mass transfer efficiency. These findings agree with previous research by Yu et al. [47], Saha et al. [49], and Xie et al. [50], all of whom observed superior desulfurization performance in finer coal fractions due to increased surface area. However, it's important to note that extremely small particles may introduce diffusion limitations, restrict the inward movement of sulfur compounds and potentially reduce microbial or chemical desulfurization efficiency in the particle's interior.

3.2.2. The effect of desulfurization on coal ash

According to Table 4, the influence of particle size on coal ash reduction exhibits a distinct pattern. The finest particle size fraction (−0.85 mm) shows the most substantial decrease in ash content—from 34.2 wt. % to 23.2 wt. %—corresponding to an ash removal rate of approximately 32.2 %, which highlights the enhanced effectiveness of microbial activity in eliminating mineral matter [46]. A further increase in temperature from 23 ± 3 °C to 30 ± 2 °C results in only a slight reduction in ash content to 23.0 wt. %, suggesting that microbial activity approaches an optimal threshold at lower temperatures, beyond which additional heat provides minimal benefit. For intermediate particle sizes, namely −2.30 + 1.00 mm and −4.60 + 2.30 mm, ash content decreases to 25.3 wt. % and 26.5 wt. %, respectively reflecting ash removal rates of 26.0 % and 22.5 %. These values indicate less effective microbial desulfurization than in the finest fraction, likely due to reduced surface area and microbial accessibility. The negligible additional ash reduction with increased temperature in these fractions reinforces the idea that surface accessibility, rather than temperature, becomes the limiting factor for microbial performance. The coarsest fraction (+4.60 mm) demonstrates the lowest ash reduction, with content decreasing to 27.4 wt. %, equating to a 20 % ash removal rate. This limited reduction is attributed to decreased surface area and restricted microbial interaction with embedded mineral matter. These findings are consistent with those of Ken and Nandi [24], who reported that larger coal particles tend to retain more mineral impurities within the coal matrix, inhibiting microbial desulfurization. Smaller particle sizes not only provide greater surface area for microbial colonization but also improve interaction with mineral-bound ash, facilitating significant reductions - as much as 33 % according to Liu et al. [26]. However, excessively fine particles may lead to diffusion limitations due to accumulation of metabolic byproducts or restricted microbial penetration

Table 4
Steady state condition experimental values.

Particle Size (mm)	Ash (wt. %) and Feed = 34.2			Sulfur Content (wt. %) and Feed =1.45			Calorific value (MJ/kg) and Feed =20.3		
	Inoculated (23 ± 3 °C)	Uninoculated (23 ± 3 °C)	Uninoculated (30 ± 2 °C)	Inoculated (23 ± 3 °C)	Uninoculated (23 ± 3 °C)	Uninoculated (30 ± 2 °C)	Inoculated (23 ± 3 °C)	Uninoculated (23 ± 3 °C)	Uninoculated (30 ± 2 °C)
−0.85	23.2	34.1	23.0	0.50	1.27	0.40	24.00	20.00	24.16
−2.30 + 1.00	25.3	34.2	25.3	0.65	1.29	0.60	22.13	20.30	22.19
−4.60 + 2.30	26.5	34.1	26.4	0.73	1.29	0.66	21.80	20.30	22.00
+4.60	27.4	34.1	27.3	1.1	1.35	1.03	21.30	20.30	21.30

[24,26]. This is evidenced by the plateau in ash removal in the −0.85 mm fraction despite temperature increase, possibly due to mass transfer constraints or microbial saturation.

Therefore, optimizing coal particle size is critical to maximizing microbial efficiency while minimizing limitations caused by reduced mass transfer or microbial inhibition. Striking a balance between increased microbial access and avoiding the negative effects of extreme fineness is key for effective biodesulfurization. In addition to microbial considerations, the high initial ash content presents significant technical challenges for coal utilization. It contributes to reduced combustion efficiency, higher operational costs in power generation, and increased environmental impact trend because of the uneven distribution of sulfur within these particles [27]. Specifically, elevated ash levels are associated with greater ash disposal requirements, boiler wall corrosion, economizer fouling, and heightened fly ash emissions [51].

3.2.3. *The effect of desulfurization on calorific value*

Table 4 illustrates that particle size variation significantly affects the calorific value of coal during biodesulfurization, following a distinct trend. The finest particle size fraction (−0.85 mm) exhibits a marked increase in calorific value-from 20.3 MJ/kg to 24.00 MJ/kg-with a further slight improvement to 24.16 MJ/kg when the temperature is raised from 23 ± 3 °C to 30 ± 2 °C. This indicates that microbial activity is most effective in finer coal particles, where enhanced surface area facilitates sulfur removal, thereby boosting the energy content of the coal. In contrast, control experiments conducted at 23 ± 3 °C without microbial inoculation showed no change in calorific value, reinforcing the role of microbial action in this transformation [46]. Intermediate particle sizes (−2.30 + 1.00 mm and −4.60 + 2.30 mm) also showed increases in calorific value, though to a lesser extent. The −2.30 + 1.00 mm fraction rose to 22.13 MJ/kg, with a marginal increase to 22.19 MJ/kg at elevated temperatures, suggesting moderate microbial effectiveness. Similarly, the −4.60 + 2.30 mm fraction increased from 20.30 MJ/kg to 21.80 MJ/kg, and then to 22.00 MJ/kg with temperature elevation, confirming that microbial desulfurization occurs but is less efficient in coarser particles.

In contrast, the largest particle size fraction (+4.60 mm) showed improvement in calorific value from 20.3 to 21.3 MJ/kg. This observation supports earlier findings that large coal particles hinder microbial access to sulfur-bearing minerals, limiting biological reactions and overall desulfurization efficiency [51,52]. Furthermore, the lack of temperature-induced improvements in this size fraction suggests that particle size, rather than temperature, is the primary factor influencing microbial activity. From a microbial interaction perspective, finer particles offer greater surface area, enhancing contact between microbes and coal and promoting more effective sulfur removal and energy enhancement. However, extremely fine particles may experience diffusion limitations, where the accumulation of metabolic by-products inhibits further microbial activity. The diminishing calorific value gain at the smallest size with increasing temperature suggests a threshold effect - beyond which microbial efficiency plateaus due to diffusion constraints. Overall, the findings confirm that desulfurized coal possesses higher calorific value than untreated coal, owing to improved organic matter content and reduced ash, aligning with the results of Liu et al. [52] and Mishra et al. [53]. The removal of non-combustible materials further enhances energy yield [53]. Thus, optimizing particle size is crucial to maximizing microbial efficiency while minimizing diffusion limitations. These observations are consistent with those of Matin and Chelgani [11], who demonstrated that specific microbial strains can selectively eliminate sulfur without compromising coal's energy content [24].

3.3. *Characterization of bacterial consortium*

The microbial community was closely monitored throughout the 20-day anaerobic desulfurization treatment. Fig. 3 illustrates the original colony morphology of the bacterial isolates from two coal particle size fractions: (a) +4.60 mm and (b) –0.85 mm. On day 20, phylogenetic trees were constructed using GenBank (NCBI) BLAST search results to provide deeper insights into the composition and diversity of the microbial community. Fig. 4 presents the phylogenetic tree, highlighting seven dominant bacterial genera identified during the treatment. These microbial communities were active within a temperature range of 23 to 30 ± 3 °C.

The seven isolates, along with their sequence query coverage percentages, were identified as follows: *I. Desulfotomaculum* (99 %), *II. Desulfosporomusa* (99 %), *III. Desulfosporosinus* (99 %), *IV. Desulforomonas* (99 %), *V. Desulfurella* (100 %),

VI. Campylobacter (100 %), and *VII. Desulfospira* (99 %). These bacteria offer promising anaerobic routes for the biological desulfurization

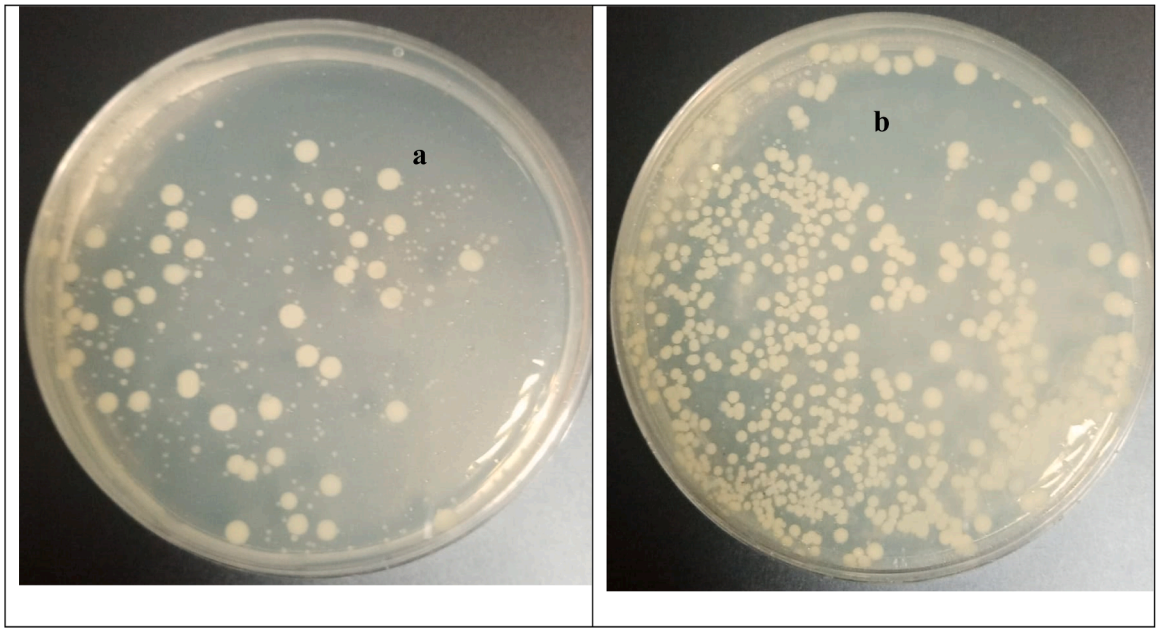

Fig. 3. The images depict the original colony morphology of the bacterial isolates (a) +4.60 mm sample, (b) –0.85 mm sample.

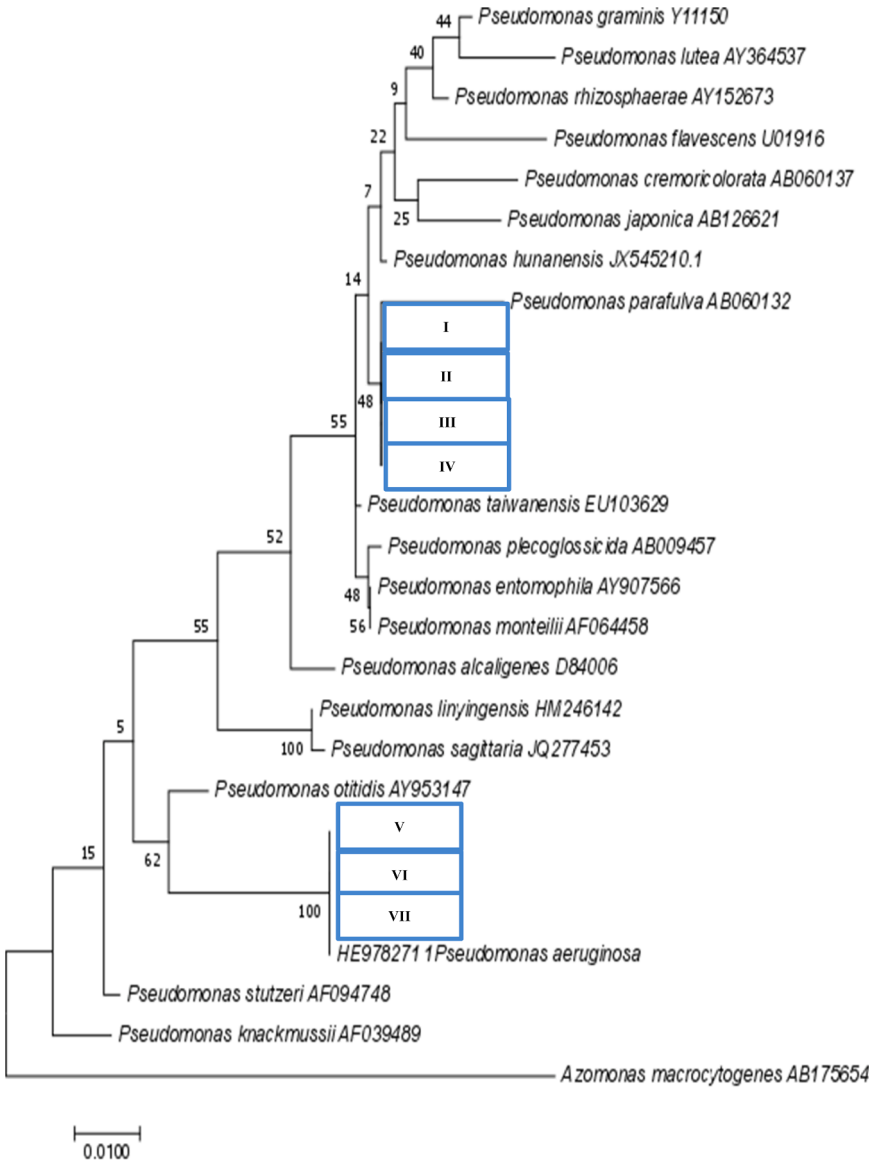

Fig. 4. A phylogenetic tree displays the major genera.

of coal. Their varying metabolic pathways, environmental tolerance, and substrate versatility support their application in diverse coal biotreatment scenarios. These bacteria are known for their capacity to degrade sulfur-containing compounds by breaking sulfur cross-links and transforming reduced sulfur species such as sulfate (SO_4^{2-}), sulfite (SO_3^{2-}), sulfide (S^{2-}), and thiosulfate ($S_2O_3^{2-}$). *Desulfotomaculum spp* can use oxygen or alternative terminal electron acceptors in their metabolic pathways, making them suitable candidates for sulfur reduction under both aerobic and anaerobic conditions [46].

The findings of this study are supported by previous research. *Desulfosporomusa spp.* for example, has been shown to effectively reduce both pyritic and organic sulfur in lignite coal [52]. Further studies by Gonsalvesh et al. [54] and Xu et al. [31] demonstrated the organism's ability to reduce organic sulfur content, thereby improving the desulfurization rate and increasing calorific value. Guo et al. [55] identified *Desulfosporosinus spp.* as another effective strain capable of lowering sulfur content in coal, while Cui et al. [56] reported that *Desulforomonas spp.* could oxidatively desulfurize compounds such as benzylmethylsulfide. *Campylobacter spp.* can be involved in partial reduction of sulfur compounds; they are not true SRBs but can play a complementary role. According to Huang et al. [46], *Desulfospira spp.* may utilize multiple metabolic pathways during the desulfurization process, including the Kodama pathway for carbon metabolism and the 4-S pathway proposed by Kilbane for sulfur metabolism. These pathways facilitate the breakdown of sulfur-bearing functional groups, such as benzenesulfonates, sulfones, and sulfoxides, resulting in water-soluble, low-molecular-weight organic by-products.

3.4. Sulfur content reduction parameters estimation

The desulfurization reaction begins through the formation of the activated complex (Coal - S.Oxidant) as an associated intermediate, as shown reaction 14:

$$\text{Coal} - -\text{S} + \text{Oxidant} \underset{\textit{Constant}\ k_2}{\overset{\textit{Constant}\ k_2}{\rightleftharpoons}} \text{Coal} - \text{S.Oxidant} \xrightarrow{\text{Constant } k_2} \text{Sulfur loss} \quad (14)$$

A dynamic equilibrium exists between the reactants and the Coal–S. Oxidant complex. In Reaction 14, this complex may either decompose into products that result in sulfur loss or revert to its original reactants. The proposed model simplifies the interpretation of Reaction 14 by

assuming the involvement of a single enzyme that facilitates sulfur removal during the biodesulfurization process. This enzymatic action leads to a reduction in sulfur content, which is mathematically expressed in Reaction 15.

$$\text{Coal} - -S_T + E \underset{\text{Constant } k_1}{\overset{\text{Constant } k_1}{\rightleftharpoons}} E * \text{Coal} \xrightarrow{\text{Constant } k_3} E + S_T \quad (15)$$

where E*Coal – S_T = The transitional bacteria-S_T complex, S_T = Sulfur content, k_1 = The reaction rate constant for the forward reaction, k_2 = The reaction rate constant for the reverser reaction, k_3 = The reaction rate constants of the third reaction, E = S_T reductase serving as a biocatalyst

Eq. (15) can represent the rate of reduction of reaction 14 if we denote the sulfur content by S_T and bacteria-S_T complex by E*:

$$\frac{dE}{dt} = k_1.S_T.E \quad (16)$$

$$\frac{dE^*}{dt} = k_2.S_T.E^* \quad (17)$$

Therefore,

$$\frac{dE^*}{dt} = \frac{dS_T}{dt} = k_3.E^* \quad (18)$$

Eq. (19) represents the rate of E* formation after combining Eqs. (16)–18:

$$\frac{dE^*}{dt} = k_1(E - E^*)(S_T) - k_2(E^*) - k_3\ (E^*) \quad (19)$$

It is fair to presume that steady-state conditions exist if E* is formed and then destroyed spontaneously in such a way that d (E*)/dt ≈ 0, as shown by Eq. (18). Thus, we can write the mass balance of Eq. (18) as follows:

$$0 = k_1(E - E^*)(S_T) - k_2(E^*) - k_3\ (E^*)$$

$$k_1S_T(E - E^*) = k_2(E^*) + k_3\ (E^*)$$

$$(k_1ES_T) - (k_1E^*S_T) = k_2(E^*) + k_3\ (E^*)$$

$$(k_1ES_T) = (k_1E^*S_T) + k_2(E^*) + k_3\ (E^*)$$

$$(k_1ES_T) = (k_1S_T + k_2 + k_3)E^*$$

Therefore, we can express E* as Eq.20 after rearranging Eq. (19).

$$E^* = \frac{S_T.E}{\left(S_T + \frac{(k_2+k_3)}{k_1}\right)} \quad (20)$$

Thus, the sulfur reduction rate in Eq. (20) becomes:

$$r = -\frac{dS_T}{dt} = \frac{k_3S_T.E}{\left(S_T + \frac{(k_2+k_3)}{k_1}\right)} \quad (21)$$

In Eq. (21), k_1, k_2 and k_3 are constant. We can replace the group of constants in Eq. (21) with a meaningful symbol from enzyme kinetics. Eq. (22) results from replacing $(k_2+k_3)/k_1$ with the half velocity concertation K_c (ML^{-3}) and k_3 with the maximum specific sulfur content reduction rate coefficient k_{mc} (T^{-1}).

$$r = -\frac{dS_T}{dt} = \frac{k_{mc}S_T.E}{(S_T + K_c)} \quad (22)$$

The rate of sulfur reduction in a biological system depends primarily on two factors: the number of active microbial cells within the reactor and the efficiency with which these cells produce sulfur-reducing enzymes across different coal particle sizes [46]. According to Huang et al. [46], the concentration of viable biomass serves as a reliable indicator of biological activity during biodesulfurization. They further suggest that cells harvested during the logarithmic growth phase can effectively substitute for enzyme E, since enzyme production is directly proportional to cell concentration, regardless of the absolute cell count [6]. Based on this relationship, the study proposes using viable biomass as a measure of biodesulfurization efficiency, which forms the basis for the development of(Eq.) 23:

$$r = -\frac{dS_T}{dt} = \frac{k_{mc}S_T.X}{(S_T + K_c)} \quad (23)$$

where: k_{mc} is the maximum specific S_T reduction rate coefficient (T^{-1}), t is the time (T), K_C is the half velocity constant (ML^{-3}), S_T is the Sulfur content at time T (ML^{-3}) and X is the concentration of viable cells at time t (ML^{-3}).

The only unidentified parameters in this model, k_{mc} and K_C, both of which exhibit stationarity with respect to X, are a result of the experiments' exceptionally high biomass concentration. X can be reasonably assumed to remain constant, as the cells were concentrated by a factor of 1 and the screening was performed under growth conditions ($X = X_o$). The analytical solution may therefore be applied to calculate the kinetic parameters, with Eq. (24) expressing the relationship as a function of time.

$$t = \frac{K_C}{X^0k_{mc}}ln\left(\frac{S_{T.0}}{S_T}\right) + \frac{1}{X^0k_{mc}}(S_{T.0} - S_T) \quad (24)$$

where, $S_{T.0\ \text{initial}}$ concentration (ML^{-3}), X^0 = Biomass concentration (ML^{-3})

A numerical solution to Eq. (24) is feasible. However, practical considerations played a significant role in the model selection process, particularly given the likelihood that multiple models could provide similarly accurate fits. To identify the most suitable parameters, Eq. (24) was optimized using experimental data processed through the AQUASIM 2.0 program. Table 5 presents the kinetic equations for sulfur content based on a Monod-type model, while Table 6 lists the corresponding kinetic parameters—k_{mc} (maximum specific reduction rate) and K_C (half-velocity constant).

The Monod equation serves as a robust tool for modeling and predicting sulfur content in coal over time or under varying process conditions. It relies on parameters estimated via nonlinear least squares regression, offering valuable insights into sulfur reduction kinetics. Statistical validity is established when the regression coefficient (R) exceeds 97 % and the square root of R^2 surpasses 95 %.The estimated biodesulfurization rate coefficient (k_{mc}) ranged from 11 to 17 h^{-1}, indicating that the highest sulfide reduction occurred during the microbial exponential growth phase. However, due to variations in coal particle sizes, it was not possible to construct a single representative kinetic model applicable across all fractions. Moreover, the K_C values obtained through nonlinear regression were inconsistent and significantly exceeded the sulfur substrate concentration ($K_C >> S_T$), a scenario in which Pan et al. [28] suggest the reaction rate approaches first-order kinetics.

A clear particle size dependence was observed. As particle size decreased, the maximum specific sulfur reduction rate (k_{mc}) increased.

Table 5
The kinetic equations for sulfur content.

Particle size	Equation
– 0.85 mm	$t = 1.039423 \times \ln\left(\frac{S_{T.0}}{S_T}\right) + 1.35933E-05 \times (S_{T.0} - S_T)$
–2.30 + 1.00 mm	$t = 1.272476 \times \ln\left(\frac{S_{T.0}}{S_T}\right) + 1.78543E-05 \times (S_{T.0} - S_T)$
–4.60 + 2.3 mm	$t = 2.111809 \times \ln\left(\frac{S_{T.0}}{S_T}\right) + 2.13894E-05 \times (S_{T.0} - S_T)$
+4.60 mm	$t = 1.8524125 \times \ln\left(\frac{S_{T.0}}{S_T}\right) + 1.620261E-05 \times (S_{T.0} - S_T)$

Table 6
The kinetic parameter estimation based on sulfur content.

Symbol	Unit	–0.85 mm	–2.30 + 1.00 mm	–4.60 + 2.30 mm	+4.60 mm
K_c	mgL^{-1}	71.271	76.465	98.731	114.328
k_{mc}	h^{-1}	17.474	14.660	13.304	11.105
R	–	0.998	0.987	0.979	0.973
R^2	–	0.997	0.976	0.956	0.962
SEE	–	0.052	1.450	1.465	2.342

#SEE: Standard Error of Estimates.

For instance, the −0.85 mm fraction exhibited the highest kmc of 17.474 h^{-1}, while the +4.60 mm fraction showed a lower kmc of 11.105 h^{-1}. In contrast, the half-velocity coefficient (K_C) increased with particle size, ranging from 71.271 mg/L at −0.85 mm to 114.328 mg/L at +4.60 mm. This inverse relationship highlights the critical role of surface area in microbial activity—smaller coal particles provide more surface area per unit mass, thereby facilitating higher sulfur reduction rates [56]. Overall, the parameter estimates for sulfur content reduction align with previous findings and reinforce the conclusion that the extent of exposed surface area is a key factor influencing desulfurization efficiency.

3.5. Estimates of parameters for ash content

Similar to the sulfur desulfurization reaction, the removal of ash content begins with the formation of an active intermediate complex, represented as (Coal–A.Oxidant), as illustrated in Reaction (25):

$$\text{Coal} - -\text{A} + \text{Oxidant} \xrightarrow[\text{Constant } k_2]{\text{Constant } k_1} \text{Coal} - \text{A.Oxidant} \xrightarrow{\text{Constant } k_3} \text{Ash loss} \quad (25)$$

The removal of ash follows a similar pathway to sulfur reduction, beginning with the formation of an active intermediate complex (Coal–A.Oxidant), as shown in Reaction (25). This study proposes that a single enzyme involved in the biodesulfurization process may also facilitate ash reduction, allowing the ash removal reaction to be simplified and represented by Reaction (26):

$$\text{Coal} - \text{A} + \text{E} \underset{Constant k_2}{\overset{Constant k_1}{\rightleftharpoons}} \text{E}^*\text{Coal} - A \xrightarrow{Constant k_3} \text{E} + \text{A} \quad (26)$$

where: E is the reductase as a biocatalyst, A is Ash, E*Coal – A is the transitional bacteria-A complex, k_1 is the reaction rate constant in forward reaction, k_2 is the reaction rate constant in the reverse reaction, k_3 is the reaction rate constants of the third reaction

Eq. (27) can represent the rate of reduction if we denote the ash value of the coal by A and the bacteria - A complex by E*:

$$\frac{dE}{dt} = k_1.A.E \quad (27)$$

$$\frac{dE^*}{dt} = k_2.A.E^* \quad (28)$$

Therefore,

$$\frac{dE^*}{dt} = \frac{dA}{dt} = k_3.E^* \quad (29)$$

Combining Eqs. (27), 28 and 29 yields the rate at which E* forms:

$$\frac{dE^*}{dt} = k_1(E - E^*)(A) - k_2(E^*) - k_3\ (E^*) \quad (30)$$

We assume steady-state conditions in the above equation, Eq. (30), as long as E* forms and breaks down on its own, such that d (E*)/dt ≈ 0. As a result, we can rewrite Eq. (30) as follows to reflect the mass balance:

$$0 = k_1(E - E^*)(A) - k_2(E^*) - k_3\ (E^*)$$

$$k_1A(E - E^*) = k_2(E^*) + k_3\ (E^*)$$

$$(k_1EA) - (k_1E^*A) = k_2(E^*) + k_3\ (E^*)$$

$$(k_1EA) = (k_1E^*A) + k_2(E^*) + k_3\ (E^*)$$

$$(k_1EA) = (k_1A + k_2 + k_3)E^*$$

Therefore, by rearranging Eq. (30), we can write E* as Eq. (31):

$$E^* = \frac{A.E}{\left(A + \frac{(k_2+k_3)}{k_1}\right)} \quad (31)$$

As a result, the rate at which ash is reduced can be calculated using 30 as follow:

$$r = -\frac{dA}{dt} = \frac{k_3A.E}{\left(A + \frac{(k_2+k_3)}{k_1}\right)} \quad (32)$$

In 30, k_1, k_2, and k_3 are constant. We can replace the group of constants in Equation 32 with a meaningful symbol from enzyme kinetics, as follows:(Eq.) 33 replaces $(k_2+k_3)/k_1$ with the half velocity concertation K_C (ML^{-3}) and k_3 with the maximum specific ash reduction rate coefficient kmc (T^{-1}).

$$r = -\frac{dA}{dt} = \frac{k_{mc}A.E}{(A + K_c)} \quad (33)$$

The quantity of active cells within the reactor and their ability to produce ash reduction enzymes significantly influence the rate of ash reduction in a biological system. Pan et al. [28] state that the quantity of viable biomass can serve as a metric for assessing the extent of biological activity during the entire operational duration. Harvesting cells during the logarithmic growth phase allows us to substitute the total amount of cellular biomass X for the enzyme E, irrespective of the number of cells X. This is because the production of the enzyme is directly proportional to the cell concentration, this is contingent upon the quantity of cells utilized at any given moment [6]. A Monod-type Eq. (34) is produced.

$$r = -\frac{dA}{dt} = \frac{k_{mc}A.X}{(A + K_c)} \quad (34)$$

where: k_{mc} is the maximum specific A reduction rate coefficient (T^{-1}), A is the Ash, (ML^{-3}), K_c is the half velocity constant (ML^{-3}), t is the time (T) and X is the concentration of viable cells at time t (ML^{-3})

The only two parameters in this model that remain unknown are kmc and K_C due to the exceptionally high biomass concentration during the trials. It can be assumed that both parameters are in a stationary phase. Given that the cells were concentrated by a factor of 1 and the screening was conducted under growth conditions, it can be confidently inferred that X remains constant, with a value equal to X_o. The analytical solution may be used to calculate the kinetic parameters. Eq. (35) expressed this as a function of time.

$$t = \frac{K_C}{X^0.k_c}\ln\left(\frac{A_0}{A}\right) + \frac{1}{X^0k_{mc}}(A_0 - A) \quad (35)$$

Table 7
The kinetic equations for ash.

Particle size	Equation
–0.85 mm	$t = 0.9578\ln\left(\frac{A_0}{A}\right) + 1.09676\ E-05 \times (A_0 - A)$
–2.30 + 1.00 mm	$t = 0.9457\ln\left(\frac{A_0}{A}\right) + 1.04599\ E-05 \times (A_0 - A)$
–4.60 + 2.30 mm	$t = 0.9022\ln\left(\frac{A_0}{A}\right) + 9.16263\ E-06 \times (A_0 - A)$
+4.60 mm	$t = 0.0700\ln\left(\frac{A_0}{A}\right) + 9.613400E-06 \times (A_0 - A)$

Table 7 presents the kinetic equations for ash values in a Monod-type equation. Table 8 displays the K_C and k_{mc} parameter estimations for ash values in a Monod-type equation. The greatest specific reduction rate coefficient for ash (k_{mc}) dropped linearly as coal particle size increased. A smaller particle of −0.85 mm had a higher maximum specific A_0 reduction rate coefficient of 17.681 (T^{-1}), whereas a larger particle of +4.60 mm had a lower maximum specific (k_{mc}) reduction rate coefficient of 11.876 (T^{-1}). However, the half velocity coefficient (K_C) increases with particle size, rising from 71.334 mg/L at −0.85 mm to 111.304 mg/L at +4.60 mm. The results for estimating the ash reduction parameter confirm the findings of Cui et al. [56], namely that the primary determining factor is the exposed coal area. It is good that the K_C and k_{mc} parameter values for ash fell within the repeatability error range. Estimating coal ash content parameters during desulfurization is crucial for optimizing the process.

3.6. Predictions of calorific values based on a variety of factors

Similar to sulfur content and ash, the desulfurization reaction for calorific value begins with the production of the activated complex (coal-CV oxidant) as an intermediate component, as shown by reaction (36):

$$\text{Coal} - -\text{CV} + \text{Oxidant} \underset{\textit{Constant}\ k_2}{\overset{\textit{Constant}\ k_1}{\longrightarrow}} \text{Coal} - \text{CV.Oxidant} \xrightarrow{\textit{Constant}\ k_a} \text{CVloss} \tag{36}$$

The Coal – CV.Oxidant and the reactants have reached a state of equilibrium. As shown in reaction Eq. (36), the Coal – CV.Oxidant breaks down either into the products, which leads to a gain in CV, or back into the reactants because it is a transient intermediate. To make modelling reaction (36) easier, we propose that a single representative enzyme, *E,* increases CV values due to the biodesulfurization treatment procedure. Thus, the reduced equation for CV improvement reads as reaction (37):

$$\text{Coal} - \text{CV} + \text{E} \underset{\textit{Constant}\ k_2}{\overset{\textit{Constant}\ k_1}{\rightleftharpoons}} \text{E} * \text{Coal} - \text{CV} \xrightarrow{\textit{Constant}\ k_3} \text{E} + \text{CV} \tag{37}$$

where: E*Coal – CV is the transitional bacteria-CV complex, k_1 *is* the reaction rate constant for the forward reaction, CV is the calorific value, k_2 is the reaction rate constant for the reverser reaction, k_3 is the reaction rate constants of the third reaction and E = CV increase by a biocatalyst. Eq. (38) can represent the rate of reduction if we denote the calorific value of the coal by CV and the bacteria - CV complex is denoted by E*:

$$\frac{dE}{dt} = k_1.CV.E \tag{38}$$

$$\frac{dE^*}{dt} = k_2.CV.E^* \tag{39}$$

Therefore,

$$\frac{dE^*}{dt} = \frac{dCV}{dt} = k_3.E^* \tag{40}$$

Table 8
The kinetic parameter estimation based on ash.

Parameter	Unit	–0.85 mm	–2.30 + 1.00 mm	–4.60 + 2.30 mm	+4.60 mm
K_c	mgL^{-1}	71.334	76.409	98.465	111.306
k_{mc}	h^{-1}	17.681	14.782	13.149	11.876
R	–	0.999	0.988	0.987	0.979
R^2	–	0.999	0.987	0.968	0.965
SEE	–	0.078	1.230	1.332	1.954

#SEE: Standard Error of Estimates.

The rate at which E* is formed can be written because of combining Eqs. (38) – 40:

$$\frac{dE^*}{dt} = k_1(E - E^*)(CV) - k_2(E^*) - k_3\ (E^*) \tag{41}$$

We assume steady-state conditions in the above equation, Eq. (41), as long as E* forms and decomposes independently, ensuring that d (E*)/dt ≈ 0. Therefore, we can rewrite Eq. (41) to accurately reflect the mass balance:

$$0 = k_1(E - E^*)(CV) - k_2(E^*) - k_3\ (E^*)$$

$$k_1CV(E - E^*) = k_2(E^*) + k_3\ (E^*)$$

$$(k_1ECV) - (k_1E^*CV) = k_2(E^*) + k_3\ (E^*)$$

$$(k_1ECV) = (k_1E^*CV) + k_2(E^*) + k_3\ (E^*)$$

$$(k_1ECV) = (k_1S_T + k_2 + k_3)E^*$$

Therefore, by rearranging Eq. (41), we can write E* as follows:

$$E^* = \frac{CV.E}{\left(CV + \frac{(k_2+k_3)}{k_1}\right)} \tag{42}$$

Therefore, we can use Eq. (42) to calculate the rate of sulfur reduction as follows:

$$r = -\frac{dCV}{dt} = \frac{k_3CV.E}{\left(CV + \frac{(k_2+k_3)}{k_1}\right)} \tag{43}$$

In Eq. (43) k_1, k_2 and k_3 are constants. We can substitute the group of constants in Eq. (43) with a meaningful symbol from enzyme kinetics, as follows: The half velocity concertation K_C (ML^{-3}) can replace (k_2+k_3)/k_1, and the maximum specific sulfur content reduction rate coefficient kmc (T^{-1}) can replace k_3:

$$r = -\frac{dCV}{dt} = \frac{k_{mc}CV.E}{(S_T + K_c)} \tag{44}$$

The rate at which sulfur content drops in a biological system depends a lot on how many active cells are in the reactor and how well they can make enzymes that lower sulfur content in different particle sizes. Liu et al. [6] propose that using viable biomass, we can estimate the level of biological activity throughout the operation. Harvesting cells during the log growth phase allows us to substitute the total cell biomass X for the enzyme E, irrespective of the number of cells, as the production of the enzyme is directly proportional to the concentration of cells. This relationship gives rise to Eq. (45), which follows a Monod-type model.

$$r = -\frac{dCV}{dt} = \frac{k_{mc}CV.X}{(CV + K_c)} \tag{45}$$

where: K_c is the half velocity constant (ML^{-3}), CV is the calorific value at time t (ML^{-3}), k_{mc} is the maximum specific reduction rate coefficient (T^{-1}), X is the concentration of viable cells at time t (ML^{-3}) and t is the time (T), the only two unknown parameters in this model are k_{mc} and K_c, both of which may be stationary with respect to X_t as the experiments were conducted under high biomass concentrations. We can safely assume that X_t is constant because we concentrated the cells by a factor of 1, and we conducted the screening under growth conditions. ($X_t = X_0$). We could use the analytical solution to calculate the kinetic parameters. Eq. (46) indicates that we wrote this as a function of time.

$$t = \frac{K_C}{X^0.k_c}\ln\left(\frac{CV_0}{CV}\right) + \frac{1}{X^0k_{mc}}(CV_0 - CV) \tag{46}$$

where: K_c is the half velocity constant (ML^{-3}), X^0 is the initial biomass concentration (ML^{-3}), k_{mc} is the maximum specific reduction rate

coefficient (T^{-1}), CV_0 is the initial CV concentration (MJ/Kg) and CV is the final CV (MJ.kg).

Eq. (46) was solved numerically, with convenience playing a key role in this choice, as multiple models could similarly fit the data. Parameter estimation was performed using AQUASIM 2.0 software to achieve the best fit between Eq. (25) and the experimental data. Table 9 presents the estimated parameters for calorific values based on a Monod-type equation, with high R^2 values (above 97 %) providing strong statistical support for the results.

The biodesulfurization rate coefficient (k_{mc}) was found to be relatively low, indicating a faster sulfur removal rate during the exponential phase. However, these characteristics did not produce a single, universally representative model applicable to all particle sizes, highlighting variability in sulfur removal rates across samples. Notably, K_C values derived from non-linear regression were variable and significantly larger than the CV values ($K_C >>$ CV). When K_C greatly exceeds S_T, the reaction rate tends to approximate first-order kinetics.

Table 9 details the kinetic equation parameters for calorific values, while Table 10 summarizes their estimations. Under first-order kinetics, the maximum specific reduction rate coefficient (k_{mc}) for CV_o increased linearly with particle size; however, the R^2 values were below 66 % for all sizes, rendering this trend statistically unreliable. In contrast, second-order kinetics revealed a higher kmc of 17.234 for the smallest particle size (−0.85 mm) and a reduced k_{mc} of 11.235 for the largest size (+4.60 mm). Additionally, the half-velocity coefficient K_C increased with particle size, ranging from 71.790 at −0.85 mm to 111.101 at +4.60 mm. All R^2 values under the second-order model exceeded 98 %, confirming strong statistical validity. Although traditional second-order kinetics refers to chemical reaction rates involving two reactants, in this case, a second-order model for calorific value uses the product of sulfur content and ash to reflect their combined effect on reducing coal's energy content. This model is best justified when data indicate that ash and sulfur together worsen coal quality more than each does individually. These results align with Cui et al. [56], who showed that the calorific value is primarily influenced by the size of the exposed coal surface. Furthermore, a strong agreement was observed between the K_C and k_{mc} parameters for ash and the repeatability errors reported for sulfur content and ash.

4. Validation of kinetic models

4.1. Sulfur content and ash model validations based on reaction order determinations

Kinetic equations based on a customized Monod-type model were developed and fitted to the experimental data for sulfur content and coal ash, as illustrated in Figs. 5–12. These graphs demonstrate that both sulfur content and ash follow a first-order kinetic model, showing strong agreement with the proposed model and supported by robust statistical evidence. For instance, the model validation for sulfur content across different particle sizes—+4.60 mm, −4.60 to +2.30 mm, −2.30 to +1.00 mm, +1.00 to +0.85 mm, and −0.85 mm—yielded high coefficient of determination (R^2) values of 0.981, 0.987, 0.978, and 0.902 respectively. Similarly, the ash model validation for particle sizes +4.60 mm, −4.60 to +2.30 mm, +2.30 to +1.00 mm, +1.00 to +0.85 mm, and −0.85 mm also demonstrated strong statistical support, with R^2 values of 0.934, 0.958, 0.966, and 0.953 respectively. These findings closely align with those reported by Ahmad et al. [57].

Table 9
Kinetic equation for calorific values.

Particle size	Equation
–0.85 mm	$t = 0.9578\ln\left(\frac{CV_0}{CV}\right)^2 + 1.09676\,E-05\times(CV_0 - CV)$
–2.30 + 1.00 mm	$t = 0.9457\ln\left(\frac{CV_0}{CV}\right)^2 + 1.04599\,E-05\times(CV_0 - CV)$
–4.60 + 2.30 mm	$t = 0.9022\ln\left(\frac{CV_0}{CV}\right)^2 + 9.16263\,E-06\times(CV_0 - CV)$
+4.60 mm	$t = 0.0700\ln\left(\frac{CV_0}{CV}\right)^2 + 9.613400E-06\times(CV_0 - CV)$

Table 10
Parameters estimation for calorific values at various coal particles.

Particle size	First-order kinetics			Second-order kinetics		
	K_c (ML^{-3})	k_{mc} (T^{-1})	R^2	K_c (ML^{-3})	k_{mc} (T^{-1})	R^2
–0.85 mm	800.22	34	0.40	71.79	17.23	0.99
–2.30 + 1.00 mm	932.48	81	0.38	76.59	14.22	0.99
–4.60 + 2.30 mm	840.11	120	0.66	98.33	13.20	0.98
+4.60 mm	945.56	201	0.43	111.10	11.24	0.97

4.2. Calorific value model validations based on reaction order determinations

The experimental data was utilized to assess the proposed model structure and its estimated parameters. As shown in Figs. 13–16, the simulated results for microbial desulfurization treatment closely match the actual data. This alignment confirms that the model's simulations generally correspond well with the experimental findings, except in Fig. 16, where the model did not accurately capture the CV profile. Fig. 16 also supports the conclusions of Makgato and Chirwa [40], who reported that reducing particle size improves sulfur removal due to an increased surface area per unit mass of coal. In contrast, larger particle sizes exhibit no clear trend because of the uneven distribution of sulfur within these particles [27,30,40]. Additionally, the half-velocity coefficient, K_C, was observed to increase with particle size, ranging from 71.790 ML^{-3} at −0.85 mm to 111.101 ML^{-3} at +4.60 mm. The coefficient of determination (R^2) values for the second-order kinetics exceeded 98 %, indicating an excellent fit and confirming the statistical validity of the results. These findings are consistent with Cui et al. [56], who demonstrated that the exposed coal surface area predominantly influences calorific value. The parameter values for K_c and k_{mc} related to ash also showed strong agreement with the repeatability errors observed for sulfur content and ash. Unlike sulfur content and ash data, the experimental CV values align well with the second-order rate equation, which is expressed in the typical quadratic form shown in Eq. (47):

$$\frac{dC}{dt} = kC^2 \tag{47}$$

where k is a constant with a specific value depending on the content of sulfur in the system.

5. Conclusions

This study provides comprehensive insights into the anaerobic biodesulfurization of coal, highlighting the significant influence of particle size, temperature, and microbial kinetics on process efficiency. Reaction rates were significantly influenced by coal particle size, with smaller particles (≤ −0.85 mm) exhibiting higher sulfur content and ash reduction rates, while larger particles (+4.60 mm) showed comparatively slower reaction rates. In the finest particle size fraction (−0.85 mm), total sulfur content decreased markedly from 1.45 wt. % to 0.50 wt. % over 20 days, corresponding to a removal efficiency of 65.5 %. Raising the temperature from 23 ± 3 °C to 30 ± 2 °C further enhanced sulfur removal, reducing sulfur content to 0.40 wt. % and achieving an overall reduction of 72.4 %. This finest particle size fraction also showed the most significant ash reduction—from 34.2 wt. % to 23.2 wt. %—

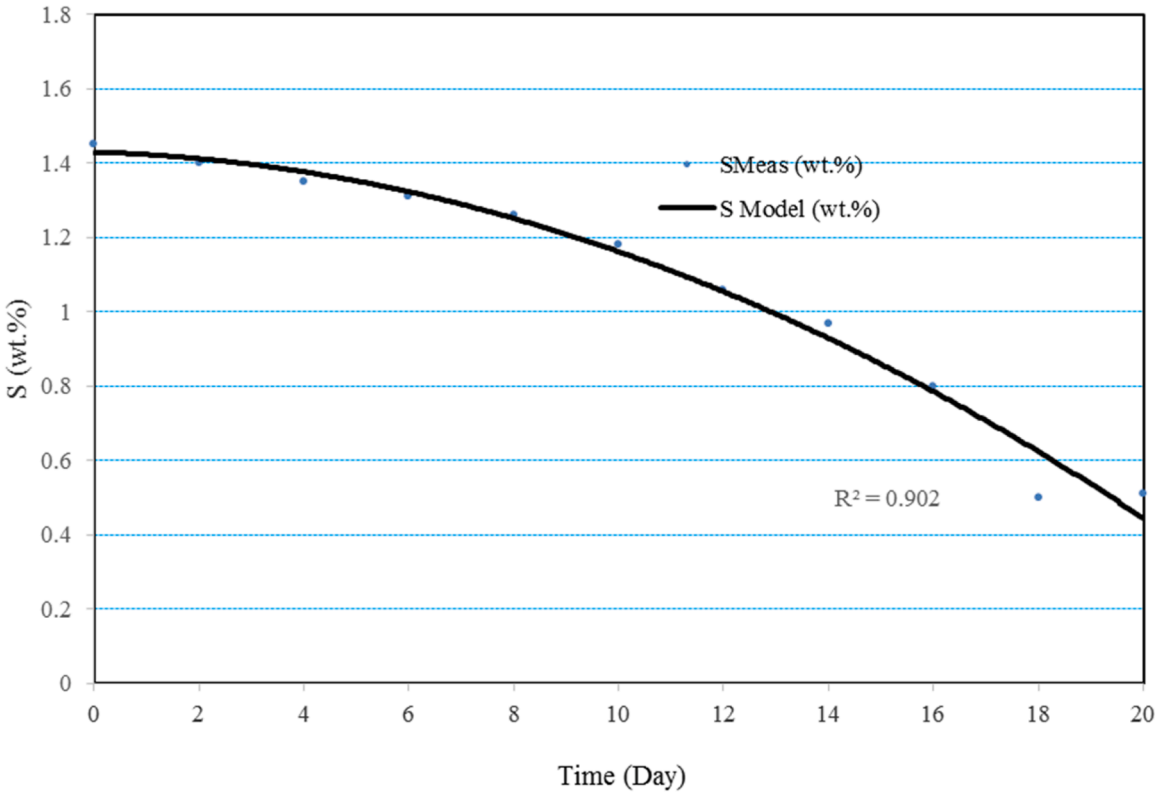

Fig. 5. The sulfur content model pertains to a coal particle size of −0.85 mm.

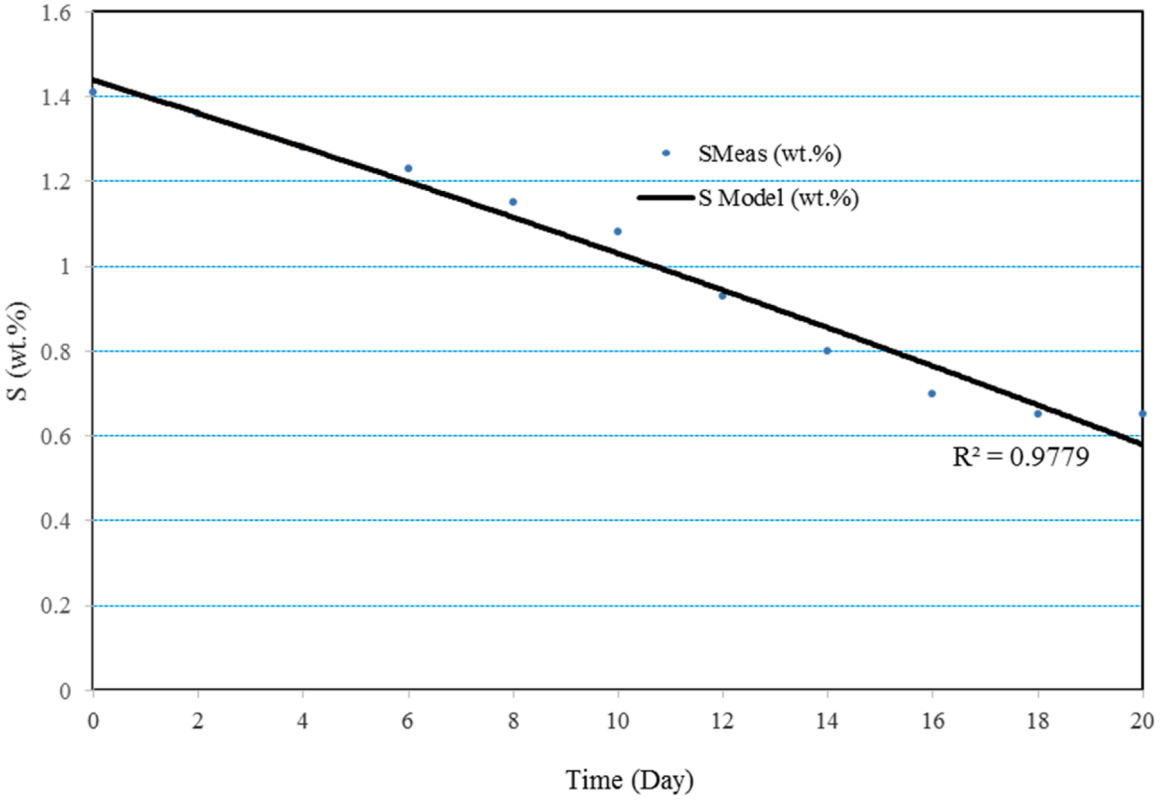

Fig. 6. The sulfur content model pertains to a coal particle size of −2.30 + 1.00 mm.

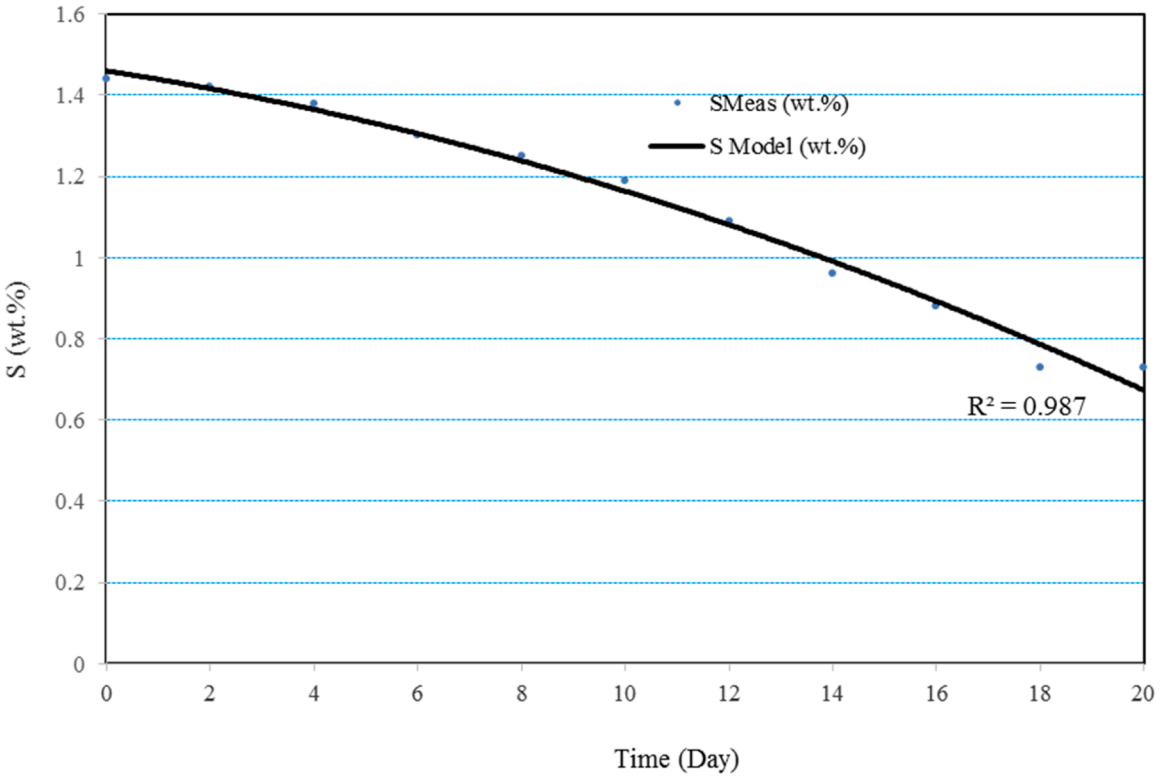

Fig. 7. The sulfur content model pertains to a coal particle size of −4.60 + 2.30 mm.

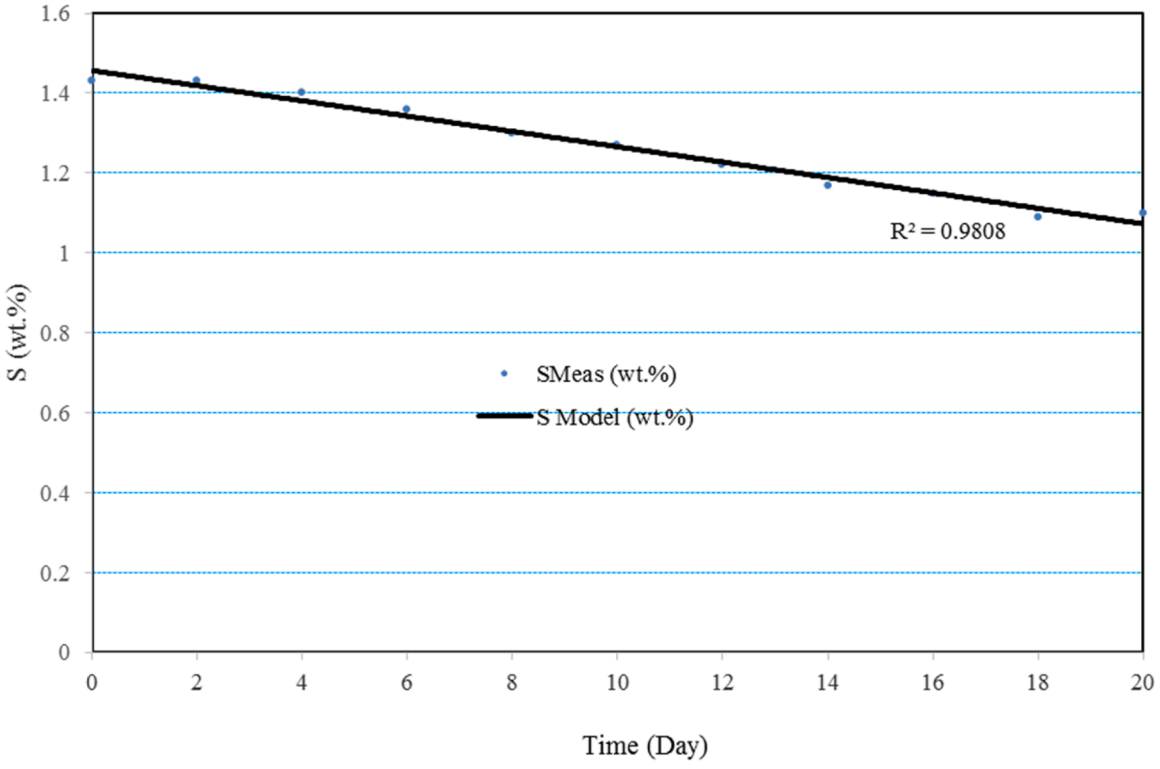

Fig. 8. The sulfur content model pertains to a coal particle size of +4.60 mm.

amounting to a 32.2 % decrease. Concurrently, the calorific value increased substantially from 20.3 MJ/kg to 24.00 MJ/kg. These improvements highlight the efficiency of microbial action in finer coal fractions, where increased surface area enhances bacterial interaction. Kinetic modeling indicated that the maximum specific reduction rate coefficient (k_{mc}) was higher for smaller particles, reflecting faster reaction kinetics. In contrast, the half-velocity coefficient (K_C) increased with larger particles, suggesting slower microbial access or reaction

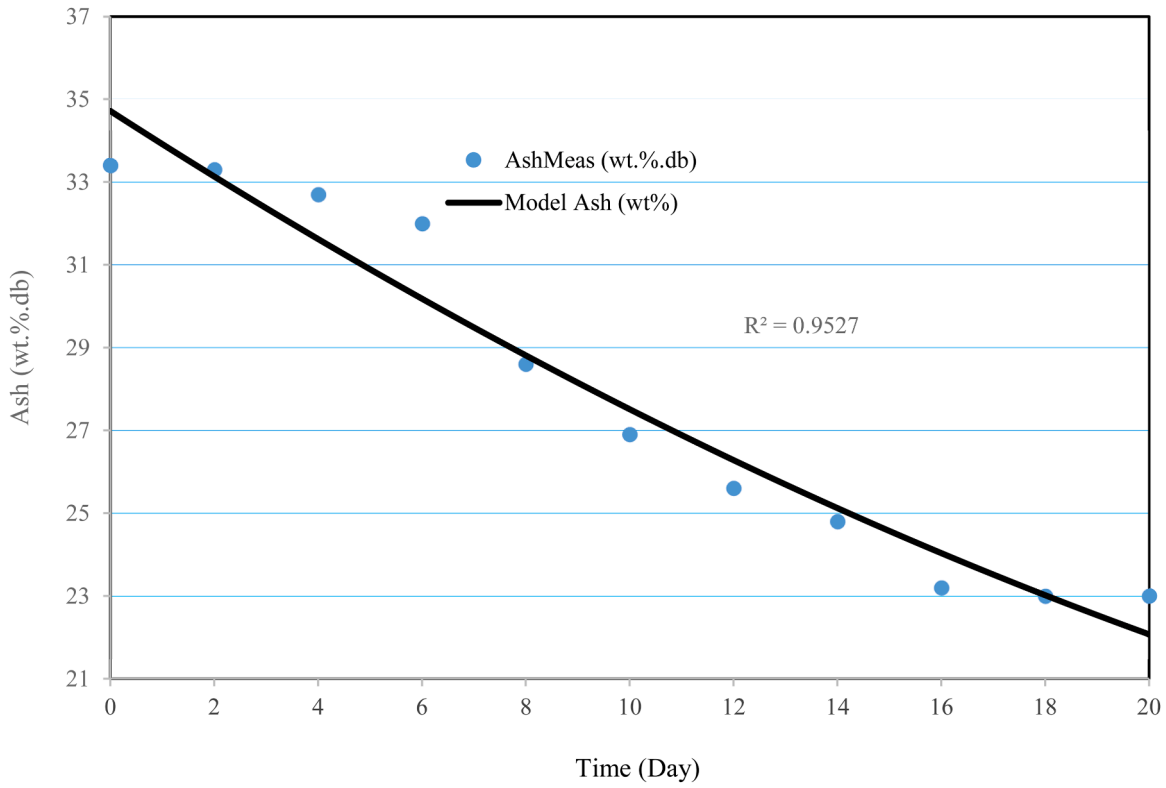

Fig. 9. The ash model pertains to a coal particle size of – 0.85 mm.

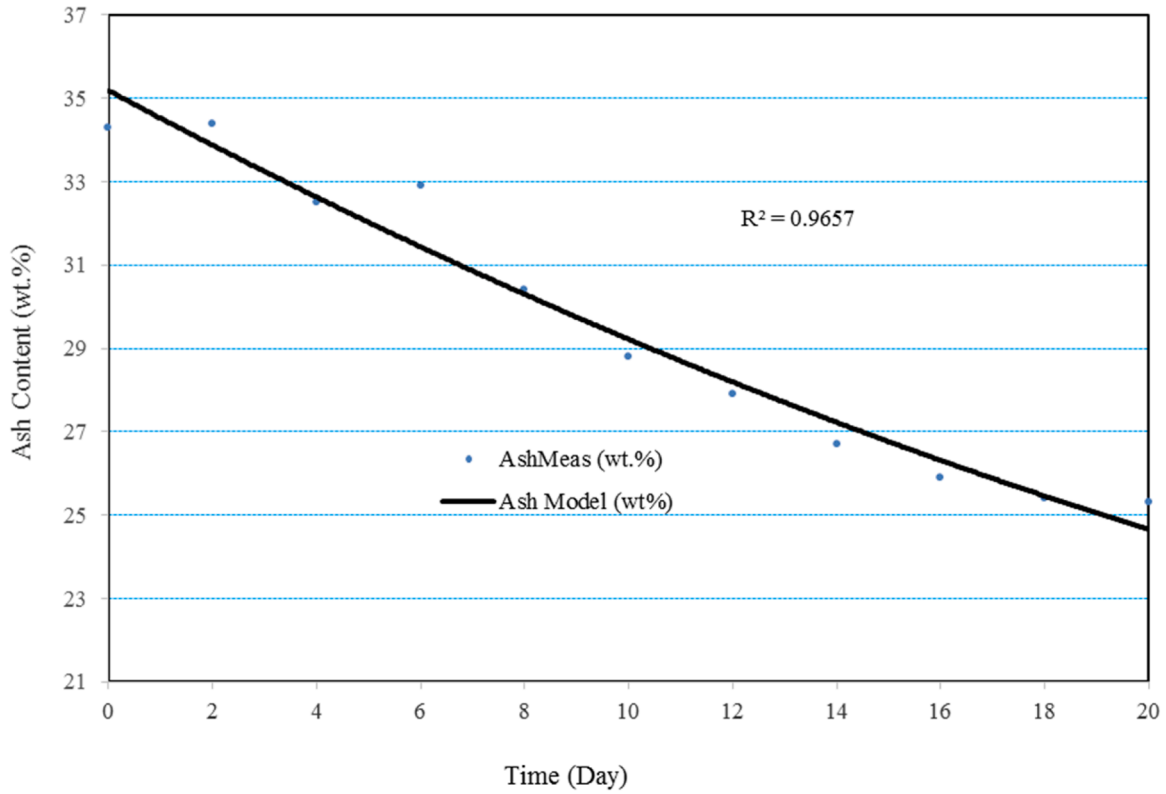

Fig. 10. The ash model pertains to a coal particle size of −2.30 + 1.00 mm.

rates. Sulfur content and ash removal followed first-order kinetics, indicating that their removal rates were directly proportional to their concentrations. Calorific value data were best described by a second-order rate equation, implying more complex dependencies. The high R^2 values (>97 %) across all models confirmed the statistical robustness of the kinetic fits. Overall, the study demonstrates that anaerobic

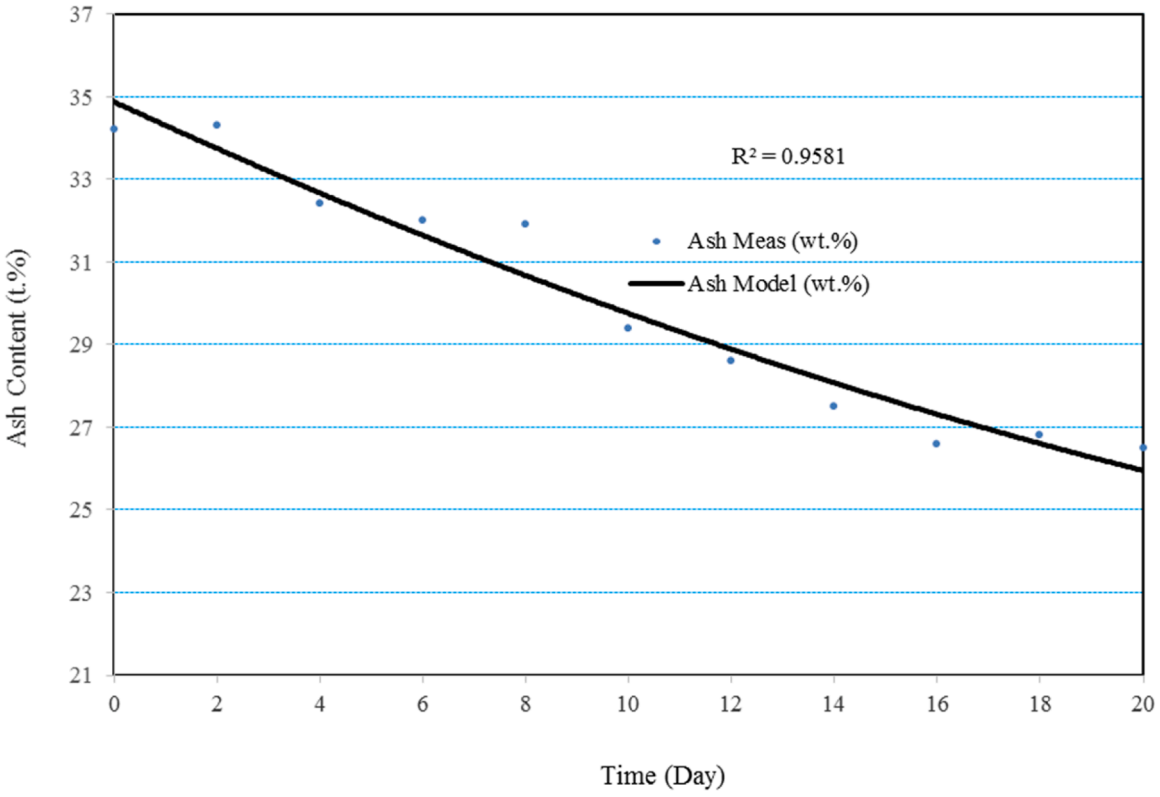

Fig. 11. The ash model pertains to a coal particle size of −4.60 + 2.30 mm.

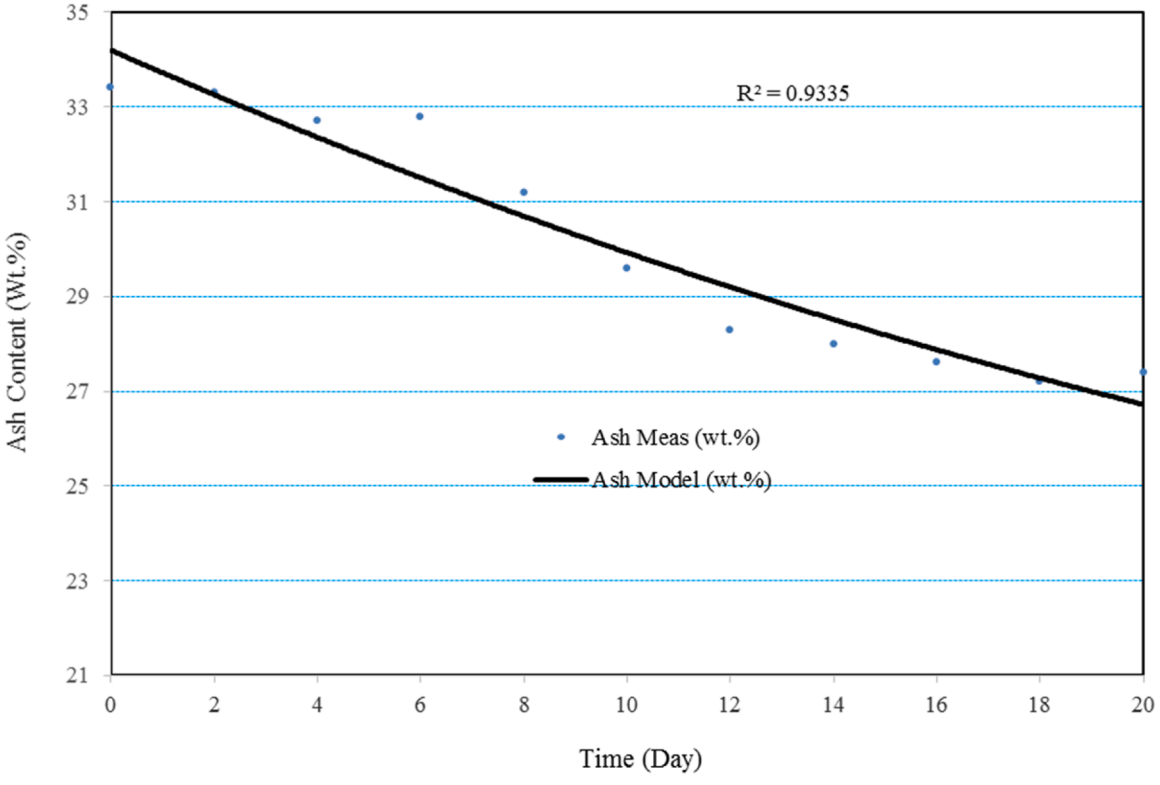

Fig. 12. The ash model pertains to a coal particle size of +4.60 mm.

bacterial consortia offer a promising, environmentally friendly approach to coal desulfurization. The findings support the development of predictive kinetic models, which are critical for optimizing process conditions. However, the broader applicability of anaerobic desulfurization depends on several factors, including coal type, sulfur forms, microbial compatibility, and operational goals. Further research is

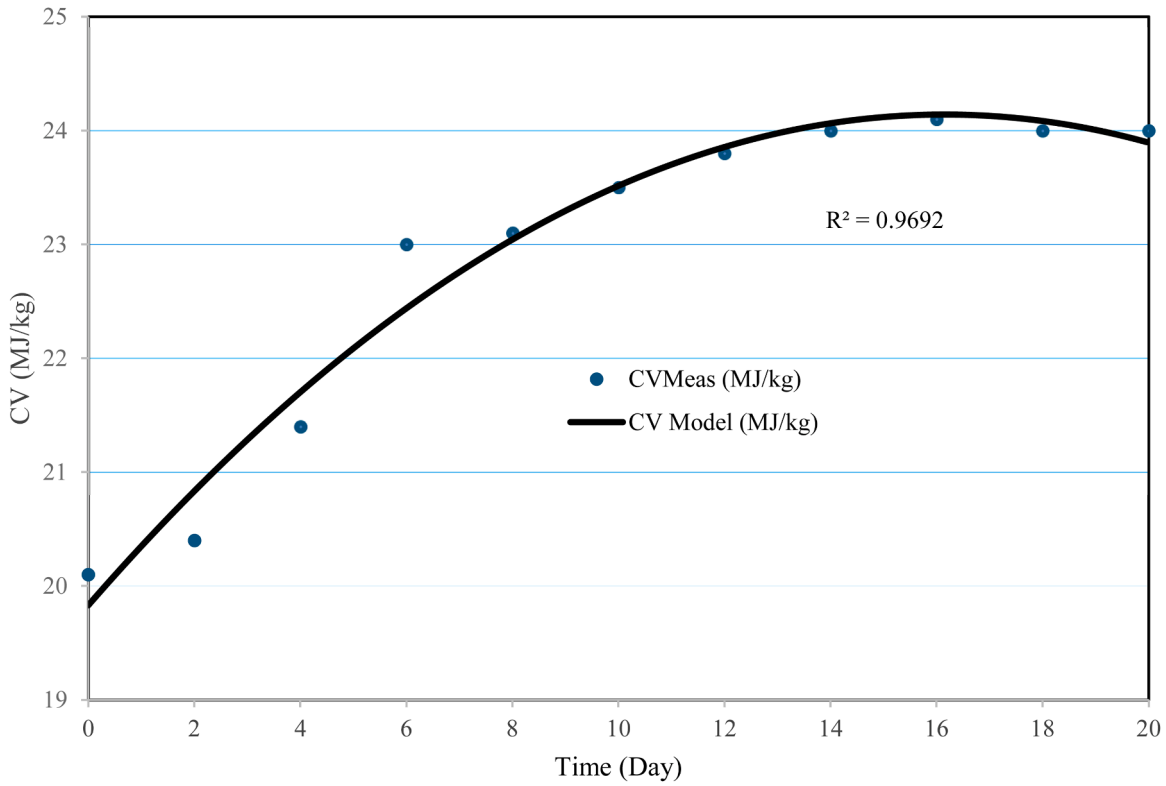

Fig. 13. Validation of the CV model for coal particles measuring −0.85 mm.

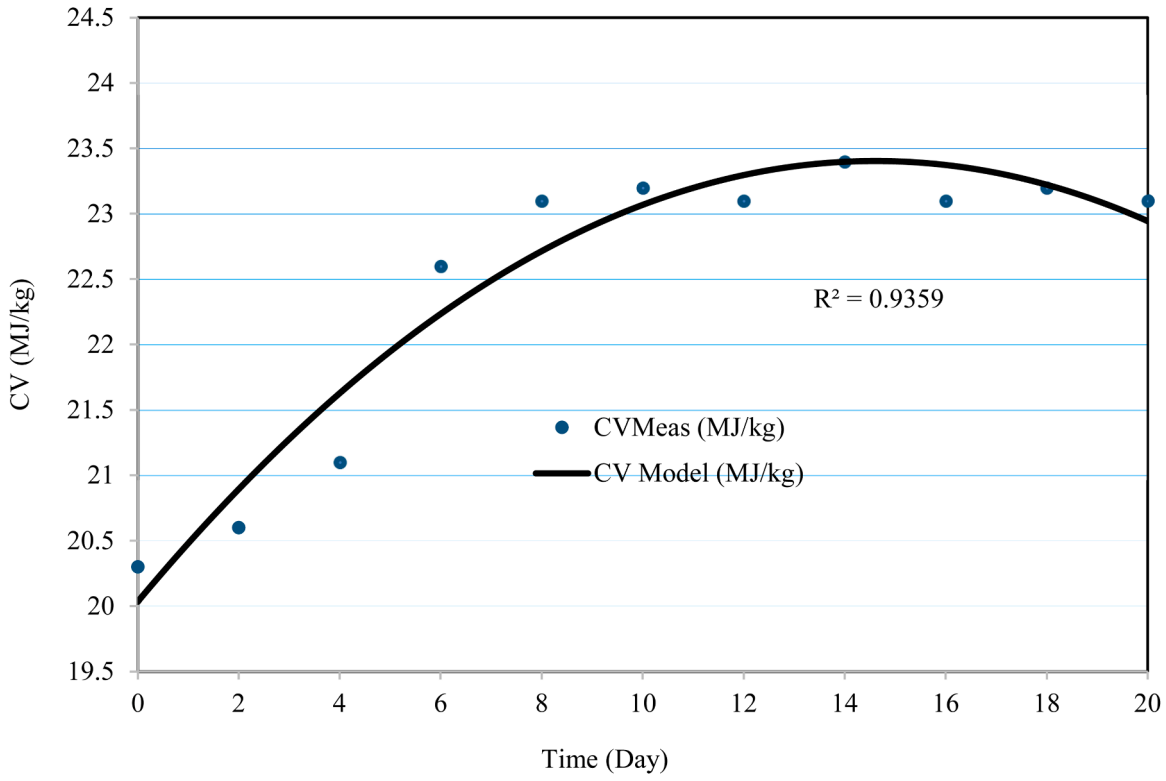

Fig. 14. Validation of a CV model for coal particles measuring −2.30 + 1.00 mm.

required to enhance process efficiency, address variability in microbial performance, and tailor kinetic models for different coal types.

CRediT authorship contribution statement

Seshibe Makgato: Writing – original draft, Methodology, Formal analysis. **Bridjesh Pappula:** Writing – original draft, Software, Formal

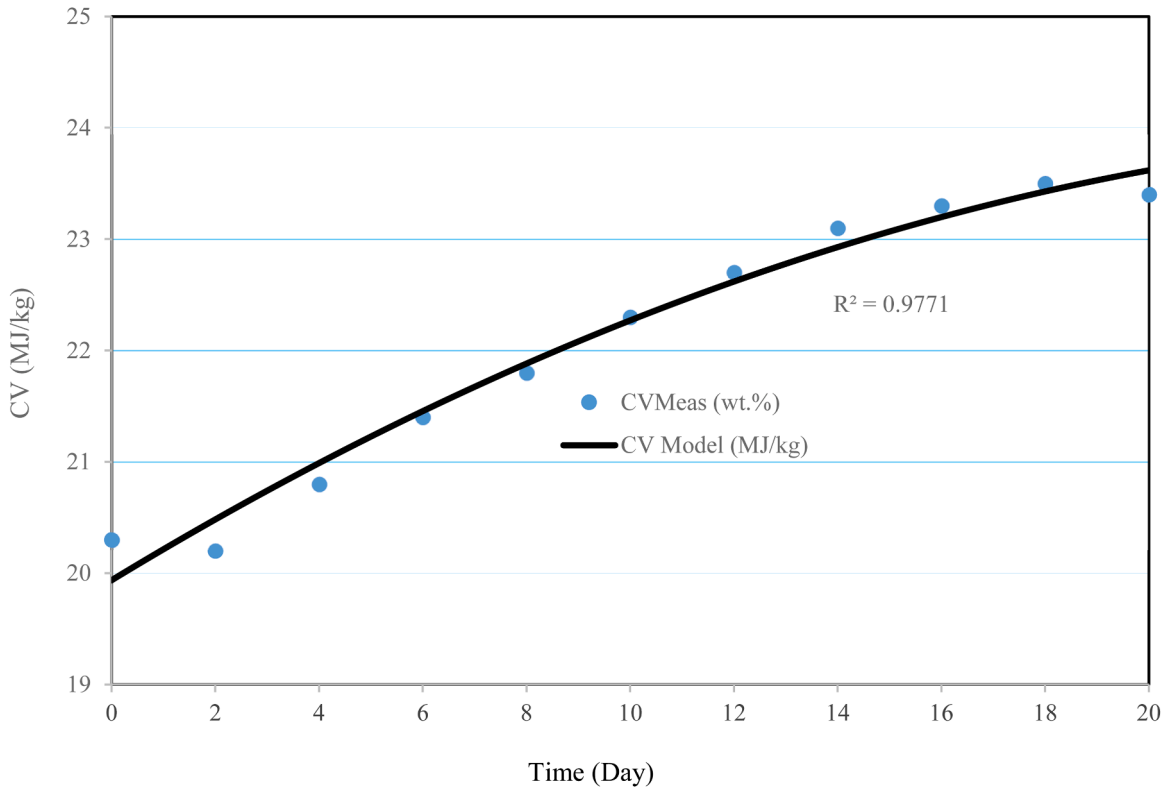

Fig. 15. Validation of a CV model for coal particles measuring −4.60 + 2.30 mm.

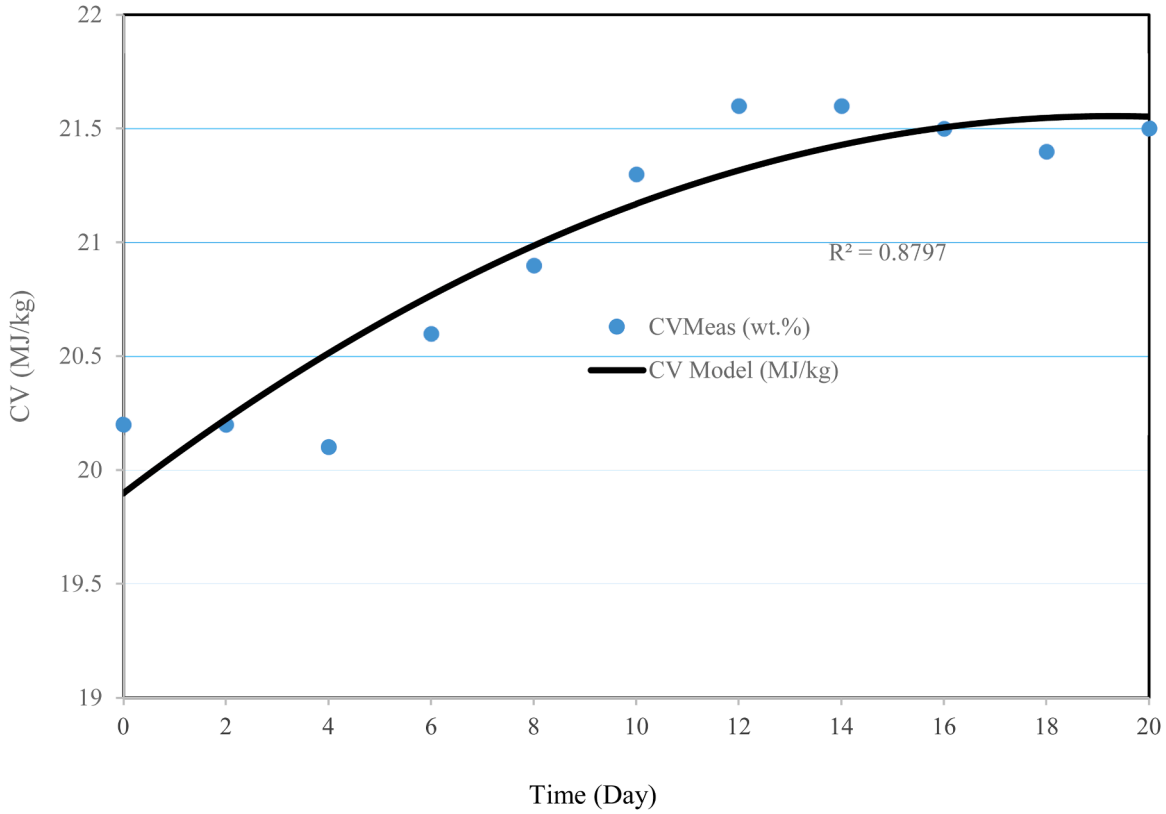

Fig. 16. Verification of the CV Model with a + 4.60 mm coal particle size.

analysis. **Opeyemi Oyewo:** Writing – review & editing, Visualization. **Tunde Yusuf:** Writing – review & editing, Methodology, Formal analysis. **Naveen Kumar:** Writing – review & editing, Project administration, Conceptualization. **Damian Onwudiwe:** Writing – review & editing, Validation, Data curation. **Peter Makgwane:** Writing – review & editing, Methodology, Investigation.

Declaration of competing interest

The authors declare that they have no known competing financial interests or personal relationships that could have appeared to influence the work reported in this paper.

Data availability

No data was used for the research described in the article.

References

[1] X. Lin, L. Fu, P. Lu, Q. Zhang, G. Xu, D. Bai, Development of a three-stage process for high coal desulfurization and char yield, J. Energy Inst. 113 (2024) 101536, https://doi.org/10.1016/j.joei.2024.101536.

[2] F.M. Nermark, R. Lindblad, M.M. Mapolelo, M. Sandahl, O.F. Wendt, C. Turner, Optimization of coal desulfurization method by sub/supercritical fluid extraction with binary mixtures of carbon dioxide and ethyl lactate as a solvent, Green Anal. Chem. 9 (2024) 100111, https://doi.org/10.1016/j.greeac.2024.100111.

[3] Y. Wu, L. Zhang, M. Liu, Z. Lei, Z. Li, W. Zhang, S. Ren, Z. Wang, H. Shui, J. Yan, Synergistic reduction of NO/SO2 through co-firing municipal sewage sludge with coal gangue, Chem. Eng. J. 496 (2024) 154025, https://doi.org/10.1016/j.cej.2024.154025.

[4] R.C. Uwaoma, C.N. Henning, J. Bunt, N.T. Leokaoke, H.W.J.P. Neomagus, Comparison of industrial wastes as a binder in the agglomeration of coal fines, Results Eng. 16 (2022) 100729, https://doi.org/10.1016/j.rineng.2022.100729.

[5] X. Yi, M. Zhang, J. Deng, Y. Xiao, X. Shi, L. Ge, Study on the effect of domesticated *Escherichia coli* on desulphurisation and spontaneous combustion oxidation characteristics of coals with varying sulphur contents, Fuel 381 (2025) 133552, https://doi.org/10.1016/j.fuel.2024.133552.

[6] F. Liu, Y. Lei, J. Shi, L. Zhou, Z. Wu, Y. Dong, W. Bi, Effect of microbial nutrients supply on coal bio-desulfurization, J. Hazard. Mater 384 (2020) 12132, https://doi.org/10.1016/j.jhazmat.2019.121324.

[7] A.M. Saleh, A.B. Alias, S.S.A.S. Hasan, A.H. Jawad, T.A. Shihab, O.M. Ali, W.A.W. A.K. Ghani, H.H. Mahdi, Ahmed OK SalehNM, Isotherm and kinetic models of SO2 adsorption on palm kernel shell-activated carbon and xerogel blends: effect of flow rate and contact time, Results Eng. 25 (2025) 103970, https://doi.org/10.1016/j.rineng.2025.103970.

[8] P. Luo, Z. Chen, X. Chen, W. Ma, X. Gan, R. Xie, Study on desulfurization and modification of high-sulfur petroleum coke via reduced iron powder catalytic roasting, J. Environ. Chem. Eng. 12 (2024) 114860, https://doi.org/10.1016/j.jece.2024.114860.

[9] C. Tong, Z. Chen, J. Cao, L. Zhu, Q. Liu, Q. Xie, Numerical simulation and optimization for the desulfurization performance inside a burner with mixed ammonia/coal combustion: a case study, Fuel 392 (2025) 134786, https://doi.org/10.1016/j.fuel.2025.134786.

[10] M. Erol, H. Haykiri-Acma, S. Küçükbayrak, Calorific value estimation of biomass from their proximate analyses data, Renew. Energy 35 (2010) 170–173, https://doi.org/10.1016/j.renene.2009.05.008.

[11] S.S. Matin, S.C. Chelgani, Estimation of coal gross calorific value based on various analyses by random forest method, Fuel 177 (2016) 274–278, https://doi.org/10.1016/j.fuel.2016.03.031.

[12] Y. Yang, X. Tao, X. Kang, H. He, N. Xu, L. Tang, L. Luo, Effects of microwave/HAc–H2O2 desulfurization on properties of Gedui high-sulfur coal, Fuel Process. Technol. 143 (2016) 176–184, https://doi.org/10.1016/j.fuproc.2015.11.023.

[13] I. Sverchkov, Determination of the calorific value and ash content of coal using the analysis of primary X-ray radiation scattering spectra, Spectrochim. Acta B: At. Spectrosc. 230 (2025) 107221, https://doi.org/10.1016/j.sab.2025.107221.

[14] K.J. Tew, R.J. Donahoe, I.G. Okunlola, Modeling the spatial distribution of REEs and Li within two coal ash impoundments, Int. J. Coal. Geol. 307 (2025) 104826, https://doi.org/10.1016/j.coal.2025.104826.

[15] W. Ahmad, M. Salman, I. Ahmad, M. Yaseen, Process for desulfurization and demineralization of low rank coal using oxidation assisted froth floatation technique, Chem. Eng. Res. Des. 205 (2024) 301–311, https://doi.org/10.1016/j.cherd.2024.03.020.

[16] Y. Li, M. He, F. Shi, High voltage pulse-enabled coal desulfurization and deashing – Part 1: selective breakdown of mineral matter, Fuel 300 (2021) 120970, https://doi.org/10.1016/j.fuel.2021.120970.

[17] L. Xue, Y. Tang, S. Gao, Structural evolution characteristics of sulfur in coal during gold-tube thermal simulation, Fuel Process. Technol. 268 (2025) 108183, https://doi.org/10.1016/j.fuproc.2025.108183.

[18] J.C. Hower, R.B. Finkelman, C.F. Eble, B.J. Arnold, Understanding coal quality and the critical importance of comprehensive coal analyses, Int. J. Coal. Geol. 113 (2022) 104120, https://doi.org/10.1016/j.coal.2022.104120.

[19] B. Ambedkar, R. Nagarajan, S. Jayanti, Ultrasonic coal-wash for de-sulfurization, Ultrason. Sonochem. 18 (2011) 718–726, https://doi.org/10.1016/j.ultsonch.2010.09.006.

[20] X. Huo, W. Zuo, F. Shi, W. Huang, Coal middling retreatment using high voltage pulse technique. Part 1: experimental findings, Fuel 314 (2022) 123066, https://doi.org/10.1016/j.fuel.2021.123066.

[21] L. Wang, X. Wen, Z. Liu, Z. Liu, Y. Zhang, X. Lu, H. Zhou, Y. Xu, Coal desulfurization by photocatalytic oxidation in the presence of [HO2MMim][HSO4] and H2O2, Fuel 306 (2021) 121754, https://doi.org/10.1016/j.fuel.2021.121754.

[22] G. Cheng, Y. Li, Y. Cao, Z. Zhang, A novel method for the desulfurization of medium–high sulfur coking coal, Fuel 335 (2023) 126988, https://doi.org/10.1016/j.fuel.2022.126988.

[23] S.K. Behera, S. Chakraborty, B.C. Meikap, Chemical demineralization of high ash Indian coal by using alkali and acid solutions, Fuel 196 (2017) 102–109, https://doi.org/10.1016/j.fuel.2017.01.088.

[24] B.S. Ken, B.K. Nandi, Desulfurization of high sulfur Indian coal by oil agglomeration using Linseed oil, Powder. Technol. 342 (2019) 690–697, https://doi.org/10.1016/j.powtec.2018.10.045.

[25] Y. Tang, L. Xue, M. Gou, L. Wang, P. Ma, X. Yu, Study on influencing factors of coal microbial flotation desulfurization, Fuel 358 (2024) 130115, https://doi.org/10.1016/j.fuel.2023.130115.

[26] J. Liu, J. Jiang, C. Jiang, Z. Wang, P. Chen, Desulfurization mechanism of high-sulfur coal by heating reduced iron powder and magnetic separation, J. Clean. Prod. 370 (2022) 133254, https://doi.org/10.1016/j.jclepro.2022.133254.

[27] S.S. Makgato, E.M. Nkhalambayausi Chirwa, Waterberg coal characteristics and SO2 minimum emissions standards in South African power plants, J. Env. Manage 201 (2017) 294–302, https://doi.org/10.1016/j.jenvman.2017.06.049.

[28] W. Pan, R. Yi, Z. Liao, L. Yang, An experimental study on enhancing microbial desulfurization of sulfide ores using ul-trasonic treatment, Mater. (Basel) 15 (2022) 2620, https://doi.org/10.3390/ma15072620.

[29] J. Tang, Y. Feng, Z. Wu, S. Zhang, E.K. Sarkodie, H. Jin, R. Yuan, W. Pan, H. Liu, Optimization studies on biological desulfurization of sulfide ore using response surface methodology, Minerals 11 (2021) 583, https://doi.org/10.3390/min11060583.

[30] S.S. Makgato, E.M.N. Chirwa, Characteristics of thermal coal used by power plants in Waterberg Region of South Africa, Chem. Eng. Trans. 57 (2017) 511–516, https://doi.org/10.3303/CET1757086.

[31] F. Xu, M. Chu, C. Hao, L. Zhou, X. Sun, Z. Gu, Volatilization characteristics and relationship of arsenic and sulfur during coal pyrolysis, Fuel 315 (2023) 123223, https://doi.org/10.1016/j.fuel.2022.123223.

[32] M. Agarwal, P.K. Dikshit, J.B. Bhasarkar, A.J. Borah, V.S. Moholkar, Physical insight into ultrasound-assisted biodesulfuri-zation using free and immobilized cells of rhodococcus rhodochrous MTCC 3552, J. Chem. Eng. 295 (2016) 254–267, https://doi.org/10.1016/j.cej.2016.03.042.

[33] Z. Kaeed, A.G. Sani, H. Najafi, M.A. Sobati, S. Movahedirad, Microwave assisted oxidative desulfurization in a helical coil reactor: CFD simulation and experimental validation, Fuel 356 (2024) 129601, https://doi.org/10.1016/j.fuel.2023.129601.

[34] ISO 12902:2001 Solid mineral fuels — Determination of total carbon, hydrogen and nitrogen — Instrumental methods.

[35] ISO 1928, 2009. Determination of gross calorific value by the bomb calorimetric method and calculation of net calorific value.

[36] ISO 157, 1996. Coal - determination of forms of sulphur.

[37] ISO 11722:2013 specifies a method for determining the moisture in the general analysis test sample of hard coal by drying in nitrogen.

[38] ISO 1171, 2010. Solid mineral fuels — Determination of ash. International Organisation for Standardization.

[39] ISO 562, 2010. Hard coal and coke - determination of volatile.

[40] S.S. Makgato, E.M.N. Chirwa, The desulphurization potential of Waterberg steam coal using bacteria isolated from coal: the SO2 emissions control technique, J. Clean. Prod. 263 (2020) 121051, https://doi.org/10.1016/j.jclepro.2020.121051.

[41] S.N. Mehdi, Z.M. Khan, H.U. Farid, S.U. Khan, M.I. Khan, M. Jameel, D. Abduvalieva, H.A. Garalleh, M. Waqas, Analyzing the combustion characteristics of Thar coal block XI: a comprehensive study, Results Eng. 24 (2024) 103038, https://doi.org/10.1016/j.rineng.2024.103038.

[42] M. Mollo, A. Kolesnikov, S. Makgato, Simultaneous reduction of NOx emission and SOx emission aided by improved efficiency of a once-through Benson type coal boiler, Energy 248 (2022) 123551, https://doi.org/10.1016/j.energy.2022.12355.

[43] Y. Xu, Y. Liu, Y. Bu, M. Chen, L. Wang, Review on the ionic liquids affecting the desulfurization of coal by chemical agents, J. Clean. Prod. 284 (2021) 124788, https://doi.org/10.1016/j.jclepro.2020.124788.

[44] C. Yue, H. Chen, L. Yan, M. Wang, L. Chang, W. Bao, J. Wang, Simultaneous analysis of sulfur and mercury occurrence forms in coal by sequential chemical extraction procedures combined with plasma low-temperature ashing and their correlation study, J. Hazard. Mater 490 (2025) 137758, https://doi.org/10.1016/j.jhazmat.2025.137758.

[45] M. Nath, P. Gopinathan, M.S. Santosh, T. Subramani, V. Ramakrishna, A.A. Khan, C.R. Ravikumarf, Exploring the potential of sulphur forms in Northeastern Indian coals: implications in environmental remediation and heavy metal sensing, Chemosphere 338 (2023) 139471, https://doi.org/10.1016/j.chemosphere.2023.139471.

[46] C. Huang, Q. Liu, X. Chen, J. Nan, Z. Li, A. Wang, Bioaugmentation with thiobacillus sp. H1 in an autotrophic denitrification desulfurization microbial

reactor: microbial community changes and relationship, Env. Res. 189 (2020) 109927, https://doi.org/10.1016/j.envres.2020.109927.
[47] X. Yu, Z. Luo, D. Gan, Desulfurization of high sulfur fine coal using a novel combined beneficiation process, Fuel 254 (2019) 115603, https://doi.org/10.1016/j.fuel.2019.06.011.
[48] J. Cheng, K. Cen, Mechanisms of strengthening energy and mass transfer in microbial conversion of flue-gas-derived CO2 to biodiesel and biogas fuels, Carbon Neutrality 1 (2022) 11, https://doi.org/10.1007/s43979-022-00004-w.
[49] M. Saha, B.B. Dally, P.R. Medwell, A. Chinnici, Effect of particle size on the mild combustion characteristics of oulverized brown coal, Fuel Process. Technol. 155 (2017) 74–87, https://doi.org/10.1016/j.fuproc.2016.04.003.
[50] W. Xie, Z. Yu, Y. He, S. Wang, L. Dong, B. Li, T. Zhang, A novel technology for the deash of fine coal by an active pulsing air separation system, J. Clean. Prod. 265 (2020) 121842, https://doi.org/10.1016/j.jclepro.2020.121842.
[51] S. Wang, J. Guo, L. Tang, H. He, X. Tao, Effect of surface roughness of Chinese subbituminous coal on the kinetics of three-phase contact formation, Fuel 216 (2018) 531–537, https://doi.org/10.1016/j.fuel.2017.12.053.
[52] T. Liu, J. Hou, Y. Peng, Effect of a newly isolated native bacteria, Pseudomonas sp. NP22 on desulfurization of the low-rank lignite, Int J Min. Process 162 (2017) 6–11, https://doi.org/10.1016/j.minpro.2017.02.014.
[53] S. Mishra, P.P. Panda, N. Pradhan, D. Satapathy, U. Subudhi, S. Biswal, B. K. Mishra, Effect of native bacteria sinomonas flava 1C and acidithiobacillus ferrooxidans on biodesulphurization of Meghalaya coal and its combustion properties, Fuel 117 (2014) 415–421, https://doi.org/10.1016/j.fuel.2013.09.049.
[54] L. Gonsalvesh, S.P. Marinov, M. Stefanova, R. Carleer, J. Yperman, Organic sulphur alterations in biodesulphurized low rank coals, Fuel 97 (2012) 489–503, https://doi.org/10.1016/j.fuel.2012.02.015.
[55] H. Guo, C. Chen, D.J. Lee, A. Wang, D. Gao, N. Ren, Coupled carbon, sulfur and nitrogen cycles of mixotrophic growth of Pseudomonas sp. C27 under denitrifying sulfide removal conditions, Bioresour. Technol. 171 (2014) 120–126, https://doi.org/10.1016/j.biortech.2014.08.035.
[56] X. Cui, S. Zhao, B. Wang, Microbial desulfurization for ground tire rubber by mixed consortium-Sphingomonas sp. and Gordonia sp, Polym. Degrad. Stab. 128 (2016) 165–171, https://doi.org/10.1016/j.polymdegradstab.2016.03.011.
[57] M. Ahmad, M. Yousaf, J.C. Han, S.U. Rahman, H.M.A. Sharif, L. Wang, Z. Tang, Y. Zhou, Y. Huang, State-of-the-art analysis of the fuel desulphurization processes: perspective of CO2 utilization in coal biodesulphurization, Chem. Eng. J. 478 (2023) 147517, https://doi.org/10.1016/j.cej.2023.147517.